DEUTSCHES ELEKTRONEN-SYNCHROTRON DESY

DESY 73/44
October 1973

Electromagnetic Interactions

by

Samuel C. C. Ting

Deutsches Elektronen-Synchrotron, Hamburg, Germany
and
Laboratory for Nuclear Science, Massachusetts Institute of Technology, Cambridge, Massachusetts, U.S.A.

2 HAMBURG 52 · NOTKESTIEG 1

ELECTROMAGNETIC INTERACTIONS

"Ettore Majorana", Erice - Trapani, July 1973

Samuel C. C. Ting,

Deutsches Elektronen-Synchrotron, Hamburg, Germany, and
Laboratory for Nuclear Science, Massachusetts Institute of Technology,
Cambridge, Massachusetts, U.S.A.

1. INTRODUCTION

These lectures will consist of three parts: A. The interaction between photons and electrons or muons. - The study of quantum electrodynamics. B. The interaction between real photons and vector mesons. - The questions on vector dominance. And C. The interaction between virtual photons and hadrons. - The question on scaling and structure functions.

2. EXPERIMENTS ON QUANTUM ELECTRODYNAMICS

On the high q^2 test of quantum electrodynamics most of the experiments are done with e^+,e^- storage rings. Most of the low q^2 test of QED has been reviewed in many international conferences and will not be discussed here. The Delbrück scattering results from DESY tests QED to very high orders and shall be discussed in detail.

None of the experiments have found any deviation from the predictions of quantum electrodynamics:

2.1 Study of $e^+ + e^- \to e^+ + e^-$: to first order two diagrams dominate:

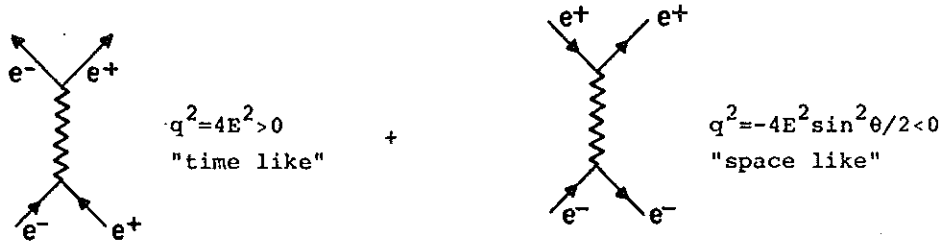

For scattering angles $\theta < 150^\circ$ - the "space like" diagrams dominate and the "time like" contributions are only few per cent.

To compare with experimental results the theoretical cross sections were corrected for radiative effects according to a formula of Tavernier[1].

This calculation uses the "peaking approximation" which predicts that the azimuthal angle between scattered particles differ from 180° by $\Delta\phi = 0$.

The experiment at the CEA[2] uses 2 GeV electron and positron beams collided head-on in a straight section of a bypass to the synchrotron. The measurement of luminosity was based on the event rate from $e^+ + e^- \to e^+ + e^- + 2\gamma$. This process is dominated by low q^2 where the validity of QED has been verified.

Figure 1 shows the detector of this experiment. It is similar to other set ups of all the first generation non-magnetic detectors in e^+,e^- storage rings. It uses spark chambers to measure coplanarity of two body events and range energy relations to identify particles.

Figure 2 shows the result of the CEA experiment compared with the predictions of QED. They find with 230 events, a $\sigma_{expt.}/\sigma_{QED} = .88 \pm .10$. One way of determining the significance of this result is to assign any possible deviation from QED to a heavy photon of mass Λ with either a positive ($\Lambda+$) or a negative ($\Lambda-$) metric. This model leads to a modification of the photon propagator by

$$F(q^2) = 1 \pm \frac{q^2}{q^2-\Lambda^2}$$

with 95 % confidence they find $\Lambda_+ > 12$ GeV, $\Lambda_- > 4.5$ GeV. If $\Lambda^2 >> 4E^2$, we find $F(q^2) = 1 \pm q^2/\Lambda\pm^2$, which is the conventional parametrization. Then the CEA results yield, with 95 % confidence, $\Lambda + > 12$ GeV, $\Lambda_- > 6$ GeV.

A precise and important experiment was done by the CERN-Bologna-Frascati group[3] at ADONE, where high statistics were obtained in $e^+e^- \to e^+e^-$ in the total c.m. energy range 1.6 GeV to 2.0 GeV. This experiment compared the angular distributions, collinearity, acoplanarity, and absolute cross sections and their energy dependence with QED to $\lesssim$1 % level. This experiment shows that peaking approximation can be applied to 2-3 % level. Figure 3 shows the $S = 4E^2$ dependence of e^+e^- events compares with prediction of QED. As seen, excellent agreements were observed. The data corresponds to their results in s = 1.44 to 9.0 GeV^2.

Taking into account experimental correction factors, the data in Fig. 3 yields an energy dependence $\sigma = (1.00 \pm 0.02)\ S^{-(199 \pm .02)}$ in good agreement with $\sigma = \frac{1}{s}$ from QED.

2.2 Study of $e^+ + e^- \to \mu^+ + \mu^-$

In this reaction only the time-like diagram contributes: comparing this reaction with $e^+ + e^- \to e^+ + e^-$ where the space-like photon dominates enables one test crossing symmetry. Or, if one assumes cross symmetry comparing $e^+ + e^- \to \mu^+ \mu^-$ with $e^+ e^- \to e^+ e^-$ checks μe universality.

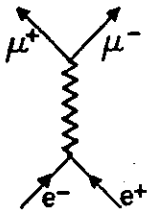

$$q^2 = 4E^2$$

Two experiments were done at ADONE. The Conversi group's[4] result is shown in Figure 4. Where R is the ratio between corrected number of $e^+e^- \to \mu^+\mu^-$ and $e^+e^- \to e^-e^+$ events from the same apparatus, plotted as a function of 2E, after normalization to the corresponding theoretical cross-sections integrated over solid angle. The dashed line responds to estimated systematic uncertainties, ignoring radiative corrections, with

$$R = \frac{[(e^+e^- \to \mu^-\mu^+)/(e^+e^- \to e^+e^-)]\text{exp}}{[(e^+e^- \to \mu^+\mu^-)/(e^+e^- \to e^+e^-)]\text{QED}} \text{ and } 400\ \mu^-\mu^+ \text{ events,}$$

and 7192 e^-e^+ events. As seen, the results agree with predictions of QED.

Quantitatively we can compare this result with the hypothesis of negative metric[5] "heavy photon" of mass m_p with

$$\frac{1}{q^2} + \frac{1}{q^2} - \frac{1}{q^2 - m_p^2}$$

The best fit of Figure 4 yields $m_p > \sim 10\ m_p$.

Alternatively we can view this experiment as a direct comparison between pure time-like process at $q^2 = 2.2 - 4.4\ \text{GeV}^2$, and essentially space-like process at $-3.5 < q^2 < -0.45$.

This will provide a check of crossing symmetry in QED with the measured $R = .96 \pm 0.065$ in good agreement with R = 1 from crossing.

A similar experiment was done by the CERN-Bologna-Frascati group[6] which compares the $e^+e^- \to e^+e^-$ $(-3.4 < q^2 < -.38\ \text{GeV}^2)$ with $e^+e^- \to \mu^+\mu^-$ $(2.56 \lesssim q^2 < 4.0\ \text{GeV}^2)$. The result shows $\mu\mu\gamma$ and $ee\gamma$ vertices are the same in agreement with other checks of μe universality. Figure 5 shows the result of this measurement. The flatness of this distribution shows that the muon behaves like electrons in

the $2.56 < q^2 < 4.0$ GeV^2 region.

An interesting experiment on $e^+e^- \to \mu^+\mu^-$ at mass of ϕ was done at Orsay[7], where they observed a deviation from the $\frac{1}{s}$ dependence of the cross section predicted from QED. A good fit to the data require one takes into account of $\gamma \to \phi \to \gamma$ transitions. Thus this experiment provides a first evidence on vacuum polarization effect.

To see this more clearly, one recalls that the Källén-Lehmann representation of the complete photon propagator.

$$D'_{\mu\nu}(K) = \frac{\delta_{\mu\nu}}{K^2} + (\delta_{\mu\nu} - \frac{K_\mu K_\nu}{K^2})\frac{1}{\pi}\int_0^\infty \frac{dQ}{Q}\frac{\mathrm{Im}\,\pi(Q)}{Q^2+K^2-i\varepsilon}$$

where $\mathrm{Im}\pi(4E^2) = \frac{E^2}{\pi\alpha}[\Sigma_f \sigma^f]$ with $\Sigma_f \sigma^f$ is the total annihilation cross section for $e^+e^- \to f$. This propagator can be tested if one chooses a pure QED process like $e^+e^- \to \phi \to \mu^+\mu^-$.

The $\sigma'(e^+e^- \to \mu^+\mu^-)$ taking into account of modification due to ϕ mesons is

$$\sigma'(e^+e^- \to \mu^+\mu^-) = \left|1 - \frac{3B}{\alpha}\frac{M_\phi \Gamma_\phi}{M_\phi^2 - 4E^2 - iM_\phi\Gamma_\phi}\right|^2 \sigma(e^+e^- \to \mu^+\mu^-)$$

with Γ_ϕ is the ϕ width, B = leptonic branching ratio $\approx 3 \times 10^{-4}$. We expect a 12 % deviation when $2E = M_\phi \pm \Gamma_\phi/2$.

The experiment was done at the Orsay storage ring with luminosity measurement by $e^+e^- \to e^+e^- + 2\gamma$ to ±5 % level and energy calibration done by detecting $e^+e^- \to \phi \to K^+K^-$. The result is shown in Figure 6. Comparing the data with σ' formula we obtain $B = (2.93 \pm 0.96) \times 10^{-4}$ in good agreement with direct result of $B = (3.01 \pm 0.12) \times 10^{-4}$. This is a direct observation of hadronic vacuum polarization.

2.3 Delbrück Scattering

A very important experiment was done recently at DESY[8] on elastic scattering of photons in the Coulomb field of nuclei via virtual electron-positron pairs. It is one of the nonlinear processes in QED which are a direct consequence of vacuum polarization. They are characterized by closed fermion loops and are forbidden via Maxwell's classical electrodynamics as a result of the linear form of its field equations and the principle of superposition The lowest order diagram is 6 order

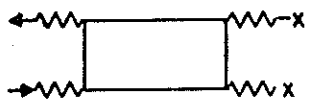

$\alpha^6 Z^4$ the next order being the 10th order

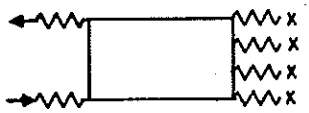

$\alpha^{10} Z^8$

It has been pointed out by Cheng and Wu[8] that in the GeV energy region the higher (>6) order diagrams make a large contribution to the measured cross sections.

By performing this experiment one checks the validity of QED to higher orders and particularly the expansion of $Z\alpha$ when Z is large.

The experiment was done with a photon beam from 1 to 7.3 GeV. Scattered photons were detected in the angular range from 1 to 3 mrad. with Cu.Au. Au. U. targets. Figure 7 shows the experimental set up of this experiment. A well collimated bremsstrahlung beam from DESY with beam divergence of ±.15 mrad, sport size 6 x 6 mm^2 hits the scattering target. The scattered photons were converted into e^+e^- pairs and measured by a pair spectrometer. The momentum resolution is ~1 %, space resolution on the pair converter was ±3 mm. The angular resolution was ±.25 mrad given by combined effect of reconstruction errors, beam spot size and beam divergence. Photon energies were measured from maximum E_o down to 0.75 E_o with 1 % resolution.

Of all the backgrounds the following 3 are most serious.

i) Compton scattering on electrons which can be calculated exactly and found to 16 % of Delbrück scattering.

ii) secondary photons from showers

iii) photon splitting 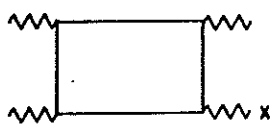

Process ii) and iii) are inelastic and do not contribute to the counting rate at the edge of the bremsstrahlung spectrum. By using 3 % wide energy band just below E_o one rejects most of these backgrounds.

Figures 8 and 9 show the result on Delbrück cross section for Au and

U targets, compared to theoretical prediction with and without Coulomb correction. The measured values are a factor 2 to 7 below the 6 orders Born approximations and are in good agreement with theory including Coulomb correction.

3. INTERACTION OF PHOTON WITH VECTOR MESONS

The physics of photoproduction of vector mesons can be visualized through the Vector Meson Dominance model[10] (VDM) where one relates the electromagnetic current of hadrons with the fields of ρ,ω,ϕ,V etc. via the relation

$$J_\mu(X) = -\left(\frac{m_\rho^2}{2\gamma_\rho}\rho_\mu(X) + \frac{m_\omega^2}{2\gamma_\omega}\omega_\mu(X) + \frac{m_\phi^2}{2\gamma_\phi}\phi_\mu(X) + \frac{m_V^2}{2\gamma_V}V_\mu(X) + \ldots\right)$$

where m_V is the vector meson mass and γ_V is the γ - v coupling strength

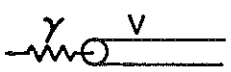

$$\frac{e\,m_V^2}{2\gamma_V} = \sqrt{\pi\alpha}\,\frac{m_V^2}{\gamma_V}$$

This model has proven to be a useful guide in understanding of many of the photon induced reactions. For example, one can relate the compton scattering amplitude to transverse vector meson photoproduction amplitude:

$$A_{\gamma p\to\gamma p} = \sum_V \frac{\sqrt{\pi\alpha}}{\gamma_V} A^{\text{Trans}}_{\gamma p\to\gamma p} \qquad (1)$$

We shall go over in detail some of the problems involved in checking the validity of (1).

We make the following observations:

i) One needs to know the coupling strength γ_V.

ii) It may require more than ρ, ω,ϕ mesons

iii) Equation (1) is an amplitude relation involving $A_{\gamma p\to Vp}$ and $A_{\gamma p\to\gamma p}$

3.1 Measurement of γ_V

The measurement of coupling constant γ_V has been carried out from DESY[11], ORSAY[12], NOVOSIBIRSK[13].

The Orsay results agree with the earlier DESY measurements and are

listed below:

	ρ	ω	φ
$\frac{\gamma_V^2}{4\pi}$	0.64±0.05	4.8±0.5	2.8±0.2

There are also very precise measurements on the forbidden decays of $\phi, \omega \to 2\pi$ by the DESY-MIT group[14] (Fig. 10). ω and ϕ are 3π resonances with $I = 0$. It decays into 2π via electromagnetic transitions of the type

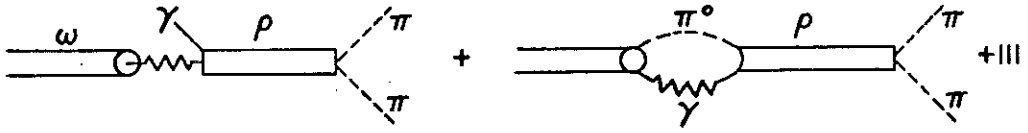

The DESY-MIT experiment measured both the production and decays of these mesons with the same apparatus and studied the non-resonant background by doing the experiment on many nuclear targets.

Their results are: $\Gamma\omega\to 2\pi/\Gamma\omega\to all = (1.22\pm0.30)$ %, $\Gamma\phi\to 2\pi/\Gamma\phi\to all = 2.7\times10^{-4}$ with 95 % confidence.

3.2 Search for new vector mesons

The first indication on the possible existence of new vector mesons at 1.6 GeV comes from the work of H. Alvensleben[15] et al. where they studied the reaction $\gamma + C \to C + \pi^+ + \pi^-$ and found a strong enhancement at mass 1.6 GeV. Figure 11 shows the result of this measurement.

Recently at Frascati[16] a 4π enhancement were observed at the same mass region from $e^+ + e^- \to 2\pi^+ + 2\pi^-$. Figure 12 shows this result. The Frascati observation implies that the enhancement is in a 1^- state.

The 4π enhancement was also observed in the Berkeley-SLAC collaboration (Figure 13) analyzing the reaction

$$\gamma + p \to p + 2\pi^+ + 2\pi^-$$

with a 9.3 GeV, $\frac{\Delta p}{p} = \pm 3$ % linearly polarized monochromatic back scattered laser beam. The experiment established that the 4π state is reached via

decay into $\rho^o + \sigma$ where σ denotes a isospin zero s-wave $\pi^+\pi^-$ system.

It should be noted that neither the $e^+e^- \to 4\pi$ nor the $\gamma + p \to p + 4\pi$ experiment can decide whether the ρ' is a resonance or a continuum. A possible way of distinction is to measure the phase of ρ' via $\gamma + p \to p\rho' \to e^-e^+$ interfering with QED pairs. Such an experiment is being performed currently at DESY.

If we interpret the ρ' being a vector meson then we have the following parameters:

i) From $e^+ + e^- \to$ pions

$M\rho' = 1.6$ GeV, $\Gamma\rho' = 0.3\text{-}0.4$ GeV

$(\frac{\gamma\rho'}{\gamma\rho})^2 \gtrsim 4$

ii) From $\gamma p \to p + 4\pi$

$M\rho' = 1.43 \pm 0.05$ GeV, $\Gamma\rho' = 0.65 \pm 0.1$ GeV

$(\frac{\gamma\rho'}{\gamma_p})^2 \gtrsim 6 \pm 2$

There are many other experiments looking for new vector mesons[18),19)]. So far the experiment has been not successful and are limited by statistics.

Two large scale experiments are being planned at Brookhaven ($p+p \to e^+e^-+X$) and at DESY ($\gamma+p \to e^+e^-+X$) to search for new e^+e^- enhancements with sensitivity down to $\sigma B \approx 10^{-38} cm^2$, and mass resolution ΔM ± 5 MeV in the mass region $1.0 < m < 6$ GeV.

To see how such an experiment is done let us look into the BNL experiment. In this experiment one uses a slow extracted 30 GeV external proton beam with intensity of 4×10^{12} per pulse. Since the invariant particle production cross section $\propto e^{-6P_\perp^*}$ and independent of $P_{//}^*$. The maximum yield is at $P_\perp^* = P_{//}^* = 0$. I.e. at rest in the c.m. system. Since particles are produced at rest, most likely it does not carry a polarization; let us look into 90^o decays.

We have

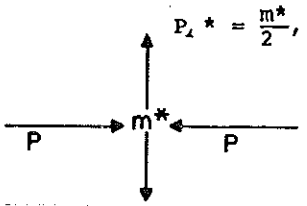

$E^* = 7.5$ GeV, m^* produced at

rest decay into e^+e^- each with $P_\perp^* = \frac{m^*}{2}$ · $P_{//}^* = 0$.
Transferred into laboratory system we have $P_\perp = P_\perp^*$; $P_{//} = \frac{m^*}{2} \cdot \frac{30}{7.5} = 2m^*$
Thus the e^+ or e^- has a laboratory emission angle of

$$\tan \theta = \frac{\frac{m^*}{2}}{2m^*} = \frac{1}{4} \text{ independent of the mass } m^*$$

A pair spectrometer with opening angle of 30^o and vertical bending to decouple P and θ is the best way to search for e^+e^- enhancement: the mass search is done by magnet exciation alone, the high incident proton beam enables us to search $V^o \to e^-e^+$ down to 10^{-38} cm^2 level.

The DESY experiment is done with a 7.5 GeV photon beam, measuring $\gamma+p \to p+e^+e^-$. It has the added advantage that one can study the phase of new e^+e^- enhancement by measuring the interference with QED pairs.

3.3 Study of the amplitude of $A\gamma p \to \gamma p$ and $A\gamma p \to vp$

3.3.1 Study of $A\gamma p \to \gamma p$

Let us now return to equation (1) and look into the physics of measuring the amplitude of compton scattering $A\gamma p \to \gamma p$. Beside the VDM equation (1) the measurement of $A\gamma p \to \gamma p$ will provide us with a direct check of the Kramers-Kronig relation[20),21)].

The measurement was carried out by the DESY-MIT group last year at DESY. This being a very difficult and important experiment, we will go into some detail of the physics, the techniques and the analysis involved.

The Kramers-Kronig relation[20)] was first derived more than 40 years ago from the causality principle. Gell-Mann, Goldberger, and Thirring[21)] obtained the same result from field theoretical considerations. It relates the real part of the forward Compton scattering amplitude, Re f_1, to the total hadronic photon nucleon cross section σ_T, via the relation

$$\text{Re } f_1(k) = \frac{-\alpha}{M} + \frac{k^2}{2\pi^2} P \int_{k\pi}^{\infty} \frac{dk'}{k'^2-k^2} \sigma_T(k') \qquad (2)$$

where P denotes the Cauchy-principal value of the integral, k_π is the one pion threshold energy, α is the fine structure constant, and M is the mass of the proton. The explicit evaluation of equation (2) has been carried out by Gilman and Damashek[22)] using the known total photon nucleon cross sections

σ_T. The purpose of this experiment is to measure Re f_1 directly and to compare it with the prediction of equation (2), thereby to check the validity of dispersion relations for photons.

The classical way to study the phase of the amplitude of πp and pp scattering is to measure the interference between the elastic scattering amplitude and the Coulomb amplitude. For Compton scattering the scattered photon, being a neutral particle, does not interfere with the Coulomb field. To study the Compton amplitude we consider the case where the scattered photon is "almost real", i.e., we study the asymmetric pair distribution from the reaction

$$\gamma + p \to p + \gamma \text{ (virtual)} \longrightarrow e^+e^- \qquad (3)$$

where the invariant mass of the pair is almost zero. To first order the amplitude for the reaction $\gamma + p \to p + e^+ + e^-$ is

$$A = A_C(\gamma) + A_{BH}(2\gamma)$$

where $A_C(\gamma)$ is the Compton amplitude with the scattered γ decaying into e^+e^-. $A_{BH}(2\gamma)$ is the ordinary Bethe-Heitler amplitude which behaves like two photons under charge conjugation. It follows from charge conjugation invariance that

$$2d\sigma_{int} \equiv |A(e^+,e^-)|^2 - A(e^-,e^+)|^2 = 4 \text{ Re } A_C(\gamma)A_{BH}(2\gamma)$$

is odd under exchange of e^+,e^-. Following Gell-Mann, Goldberger, and Thirring, we write the forward Compton amplitude

$$A_C = f_1 \vec{\varepsilon} \cdot \vec{\varepsilon}' + i f_2 \vec{\sigma}\cdot\vec{\varepsilon} \times \vec{\varepsilon}'$$

where $\vec{\varepsilon}$ and $\vec{\varepsilon}'$ are the polarization vectors of initital and final photons, respectively. If we average over nucleon spins in the amplitude, we are left with f_1. At $t = 0$, or in forward direction, the imaginary part of f_1, Im f_1, is Im f_1 $(k) = (k/4\pi)\sigma_T(k)$, and the real part of f_1 is related to the Im f_1 via equation (2).

Since the interference cross section $d\sigma_{int}$ is asymmetrical under interchange of 4-momenta of electron (P_-) and positron (P_+), it can be observed by taking the difference between two yields, N_+ and N_-, for settings of opposite polarity of an asymmetric detector. The resultant yield is then independent of the Bethe-Heitler and Compton yields. The contribution from

higher order diagrams has been estimated by Brodsky[23] and been found to be small compared to the interference term, $d\sigma_{int}$, and has been neglected.

To compare the results with the dispersion relation calculation directly, the following facts should be noted:

i) The scattered photon has to be "almost real", i.e., the electron-positron pair's invariant mass should be close to zero.

ii) The momentum transfer to the recoil proton has to be very small. $-t \leq m_\pi^2$

iii) The incident photon energy should be well above the nuclear resonance region.

These conditions are the main experimental difficulties. One is forced to study zero opening angle electron-pairs near the forward direction, where the single arm electron rate is greater than the pair rate by a factor 2×10^4. The accidental coincidence rate becomes a serious problem.

Figure 14a shows the schematic of the double arm spectrometer, where MA, MD_1, and MD_2 are large aperture dipole magnets. RF, RB, R1, R2, R3 etc. are scintillation counters, RC and LC are threshold Cerenkov counters and LS and RS are lead lucite shower counters used to distinguish pions from electrons. QM is a specially built small quantameter which provides the clearance for forward e^+e^- to enter the spectrometer.

The incident beam with k_{max} = 3 GeV and an intensity of 2×10^9 equivalent quanta per second had a sport size of 6x6 mm^2. The beam was defined by two adjustable collimators and cleaned of charged particles by bending magnets.

In order to minimize accidentals it was desirable to run the experiment at low intensities. The large acceptance of the spectrometer allowed us to do so and still obtain a sufficient event rate. We had Δk = 1 GeV, Δt = 0.025 $(GeV/c)^2$ (FWHM), $\langle k \rangle$ = 2.2 GeV and $\langle t \rangle$ = -0.027 $(GeV/c)^2$.

The acceptance of the spectrometer was defined by scintillation counters alone. To reduce dead time of the system to the percent level, the "hottest" counters LF, RF, LB, RB were split into hodoscopes. The rates in each hodoscope were about 300 kHz. Additional hodoscopes at locations R1, R2, R3 were used to determine the kinematics of each event.

To reduce the background from the reaction

$$\gamma + p \longrightarrow X + \pi^0 \longrightarrow e^+e^- \qquad (4)$$

which peaks strongly at zero opening angles, the mass acceptance of the spectrometer was deisgned to peak at 25 MeV with Δm = 20 MeV (FWHM).

To control the accidentals, the triggering time of each counter was measured separately by a time-of-flight system. Thus we could determine time distributions of accidentals in each arm separately ("single arm accidentals") as well as distributions of double arm accidentals. Because of the large acceptance of the spectrometer, neither first nor second order transport equations could be used; instead, a three dimensional magnetic field mapping of the spectrometer was made and quadratic interpolation methods were used to calculate the acceptance. The accuracy of this calculation was further confirmed by floating wire measurements.

During the experiment many checks were made to monitor the functioning of the spectrometer. We list the following examples:

i) The spectrometer polarities were reversed every 3 hours. A proton resonance meter was used to ensure that the magnetic field returned to 1 part in 10^4 of the designed value. The single arm rates were recorded continuously and found to be reproducible to 1 %.

ii) To ensure that the acceptance of the spectrometer was really defined by counters, we sytematically moved the shielding away from the accepted region by 2.5 cm. To an accuracy of 1 % no detectable effects were found.

iii) Target out rates were measured and were found to be approximately 3 %.

iv) The stability of the quantameter, the hydrogen target and the incident beam direction were monitored by a pair of spectrometers looking at the H_2 target (Fig. 14a). The rate was constant to 1 % with respect to the flux measured by the quantameter.

Half the data were taken at each spectrometer polarity. These yields are denoted as N_+ and N_-. 14b shows the time-of-flight spectrum of all the detected electron pairs. As seen, most of the events are contained within

1.2 ns. The accidentals outside the peak were equal for both polarities. They do not contribute to the observed asymmetry $N_+ - N_-$. The smallness of the accidental background in Fig. 14b enables one to subtract the accidentals with confidence. The validity of the background treatment was checked by analyzing the asymmetric yield $N_+ - N_-$ without background subtraction. Our final result was not significantly changes. Fig. 14c shows the total event distribution $N_+ + N_-$ as a function of mass.

The solid line in Fig. 14c is a theoretical yield of e^+e^- pairs. For pair mass below 20 MeV, a systematic uncertainty of ±30 % comes mainly from uncertainty in the cross section for reaction (4). For invariant mass greater than 20 MeV the contribution comes almost completely from QED pairs, for which the systematic error is small. The agreement between theory and experiment indicates that all systematic uncertainties have been understood and taken into account. The spectrum shown in Fig. 15a can be compared directly with the predictions of dispersion relations. The solid line in Fig. 15a is a dispersion relation calculation following Gilman and Damashek. The data of Fig. 15a yield a value for the real part of the Compton amplitude of -12.3±2.4μb·GeV.

As seen in Fig. 15b, this value agrees well with the dispersion calculation as a function of k.

3.3.2 Study of $A\gamma p \to Vp$

Let us look into the measurement of $A\gamma p \to Vp$ of Equation (1). Up to now most of the measurements are of the type

$$\gamma + p \to V^o + P$$
$$\qquad\qquad\quad \downarrow$$
$$\qquad\qquad\quad \text{hadrons}$$

to obtain the cross section for photoproduction of vector mesons and checks of vector dominance are made by square both sides of equation (1). The comparison on both sides of Equation (1) are difficult to make because the cross section from $\gamma + p \to V^o + P$ (with $V^o \to$ hadrons) are model dependent on the mass m_V, width Γ_V, the shape of the resonance R (m), and the analytical form of the nonresonant backgrounds assumed.

For $\gamma p \to \rho p$: In using the reaction $\gamma + p \to \pi^+\pi^- + p$ to obtain $\gamma + p \to \rho^o + p$ cross section one commonly assumes two kinds of nonresonant backgrounds.

a) The Soding type background with photon split into 2π and one π elastically scatters off nucleon. The 2π are in a p state and interfere with the $\rho \to 2\pi$ amplitude to produce the observed mass spectrum. The difficulty with this model being on how to avoid the double counting problem of distinguishing the 2π in the p state from $\rho \to 2\pi$ amplitude.

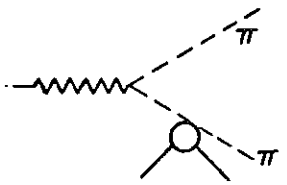

b) The other more phenomenological approach is to assume the $\gamma+p\to\pi\pi p$ spectrum are all from $\rho \to 2\pi$ and the $\rho \to 2\pi$ spectrum has a $(\frac{m_\rho}{m_{\pi\pi}})^{n(t)}$ factor in it. The two approaches can yield cross sections which differ from each other by 30 % or more[24].

For narrow resonances like $\gamma + p \to \omega + p$ and $\gamma + p \to \phi + p$ the background problems are much less (<10 %) and a reasonable model independent analysis of the data can be made and the data yields:

For $\gamma + p \to \omega + p$: The total cross section can be separated into contributions σ^N, σ^U form natural and unnatural parity exchanges in t channel.

$$\sigma^{N,U} = \frac{1}{2}\,(1 \pm P_\sigma) \cdot$$

The data[24] (Fig. 16) shows that σ^U decreases rapidly (E_γ^{-2}) with increasing energy while σ^N is approximately constant.

For $\gamma + p \to \phi + p$: This reaction is thought to proceed only by Pomeron exchange in the t-channel. Fig. 17 shows the differential cross sections[24),25] and the observed slope is $\sim$4 GeV^{-2} smaller than the ρ, and ω production slopes. The integrated cross section is shown in Fig. 18. As seen, the production cross section may increase slightly with energy.

Finally we discuss the "best way" to study photoproduction cross section and the photoproduction phase of vector mesons:

With the reaction

$$\gamma + p \to p + V^o \quad (V^o \to e^+e^-)$$

measuring e^+, e^- and recoil protons will enable us to reject all the inelastic contributions of the type $\gamma + p \to \rho + N^*$. As discussed earlier, the total amplitude comes from $A = A_{BH}(2\gamma) + A_{VP}(\gamma)$ with $|A_{BH}(2\gamma)|^2 \sim \frac{1}{\theta^8}$, $|A_{VP}|^2 \sim \frac{1}{\theta^4}$

where θ is the opening angle in the laboratory with respect to incident direction. When $\theta \to$ large $|A_{BH}(2\gamma)|^2 \to$ small and can be calculated exactly, and there are no other backgrounds. The interference term $|A(e^+,e^-)|^2 - |A(e^-,e^+)|^2 = 4A_{BH}$ Re A_{vp} measures the phase of $A_{\gamma p} \to vp$. Thus for a wide enhancement like ρ' the phase measurement is the only way to distinguish it from a real resonance.

4. ELECTROPRODUCTION

The electroproduction data will be discussed in terms of the standard variables:

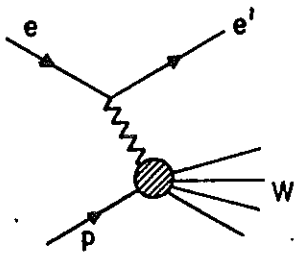

$e = (\vec{e},E)$, $e' = (\vec{e}',E')$	four momenta of the incoming and scattered electrons
$\theta =$	e' scattering angle in the Lab. system
$p = (0,m_p)$	target proton
$-Q^2 = (e-e')^2 = -4EE' \sin^2 \frac{\theta}{2}$	mass squared of virtual photon
$\nu = E - E'$	Lab. energy of virtual photon
$W^2 = (e-e'+p)^2 = 2m_p\nu + m_p^2 - Q^2$	mass squared of outgoing hadron system

For virtual photons $(-Q^2) < 0$ the photon polarization vector has a transverse as well as a longitudinal component. The differential cross section for electroproduction, $d^2\sigma/dQ^2dW$, can be expressed in terms of the cross sections σ_T and σ_L for scattering of transverse and longitudinal photons:

$$\frac{d^2\sigma}{dQ^2dW} = \frac{\pi}{EE'} \frac{W}{m_p} \Gamma_T \{\sigma_T(Q^2,W) + \varepsilon \sigma_L(Q^2,W)\}$$

with the transverse flux, Γ_T, being defined as

$$\Gamma_T = \frac{\alpha}{E\pi^2} \frac{E'}{E} \frac{W^2 - m_p^2}{m_p Q^2} \frac{1}{1-\varepsilon}$$

and $\varepsilon = \left[1 + 2(Q^2 + \nu^2)\, Q^{-2}\, tg^2\, \frac{\theta}{2}\right]^{-1}$

In terms of structure functions W_1, W_2 we have

$$\frac{d\sigma'}{dWdQ^2} = \sigma_{mott}\, \{W_2 + 2\, \tan^2\, \frac{\theta}{2}\, W_1\} \quad \text{with} \quad \sigma_T \overset{\sim}{\sim} \frac{\nu W_2}{Q_2} \underset{Q^2 \to 0}{\to} \sigma_{\gamma p}(s)$$

Much of the experimental work at electron accelerators is now concentrated on the study of inelastic electron and muon scattering in an effort to understand the cross section observed in the deep inelastic region[26),27)]. While the nucleon electromagnetic formfactors fall rapidly with Q^2 the total inelastic ep scattering cross section decreases only slowly with Q^2 (see Fig. 19) and appears to have a pointlike behaviour. There are now experimenters to measure individual inelastic channels in order to see whether the observed Q^2 behaviour is caused by specific final states.

4.1 Electroproduction of vector mesons

There are two main interests in the electroproduction of ρ^o mesons:

i) VDM relates $\gamma_v + p \to \rho + p$ with the virtual compton scattering $\gamma_v + p \to \gamma_v + p$ and through optical theorem to the total inelastic cross sections, and

ii) It has been suggested[28)] that the hadronic interaction radius of the photon shrinks as Q^2 increases.

Figure 20 shows the result for $e + p \to e + p + \pi^+ + \pi^-$ as a function of W in different Q^2 intervals[29)]. Qualitatively the same W dependence is observed in photoproduction[30)]. The Q^2 dependence of the cross section for $ep\pi^+\pi^-$ is approximately the same as that of total inelastic cross section (Fig. 21).

To study the cross section for $e + p \to e + p + \rho^o$ from $e + p \to e + p + \pi^+\pi^-$ one encounters same uncertainties as for photoproduction. And again in the absence of any reliable theory, one tries to fit the $\pi^-\pi^+$ spectrum with a relativistic Breit-Wigner with a p wave width, multiplying by a generalized mass shift factor

$$\frac{(m_\rho^2 + Q^2 - t)^2}{(m_{\pi\pi}^2 + Q^2 - t)^2}$$

No attempts to solve the problem of ρ-ω interference has yet been made, and Fig. 22 summarizes the various measurements of the diffractive slope for $\gamma_V + p \to (\rho, \omega) + p$ [31] plotted against the dimensionless inverse lifetime parameter $\frac{Q^2+m_\rho^2}{2M\nu}$. The data indicate that the slope decreases to less than half of its photoproduction value.

A decrease in slope has been predicted for electroproduction as the photon makes the transition from $Q^2 = 0$ where it has an effective hadronic "size" determined by its virtual vector meson components, to large space like Q^2, where the life time $\Delta\tau = (E_\rho - \nu)^{-1} = \frac{2\nu}{(Q^2+m_V^2)}$ of the vector meson state becomes short and the photon-proton interaction becomes more pointlike.

4.2 Multiplicities of Charged Hadrons

The data (Fig. 23) from 16 GeV SLAC track chambers [32] shows that the average multiplicity scales with $\omega' = 1 + s/Q^2$ for $|Q^2| > 1$ GeV.

4.3 Inclusive Particle Spectra

Several experiments have been focused on the Q^2 variation of inclusive π, k, p momentum and angular spectra. The results are usually presented in terms of the transverse momentum P_T and the Feynman variable $x = P_{\parallel}^*/P^*_{max}$ where $P_{\parallel}^*$ and P^*_{max} are the longitudinal and maximum possible momentum in the cms for the particle in question. All quantities refer to the process

$$\gamma_{\text{virtual}} + P \to \text{hadrons}$$

At high energies we expect to find three distinct x regions with qualitatively different behaviour:

$x \approx -1$ particles from target fragmentation

$x \approx +1$ particles from beam fragmentation

$x \approx 0$ central region with particles coming - in terms of the multiperipheral model - from the middle rungs.

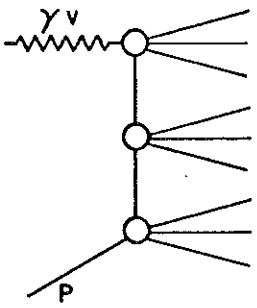

beam fragmentation

central region

target fragmentation

With this picture in mind we expect e.g. the pion distribution in the target region to be independent of the nature of the beam particle. Applied to electroproduction, at large energies the pion distribution for $x < 0$ should not depend on Q^2.

4.3.1 π Spectra: Fig. 24, 25, 26 showed the π^+, π^- distribution integrated over P_T for given Q^2 intervals for DESY and SLAC energies, and we observe that:

i) for $X < 0.3$ the data is independent of Q^2

ii) for $X > 0.3$ the data is decreasing with increasing Q^2.

The $X > 0.3$ data is namely from two body channels like ρ^o production and $\gamma_v p \to \pi^+ n$, $\pi^+ \Delta^o$, $\pi^+ N^*$ (1520)

4.3.2 K Spectra: The limited data on the inclusive K^+ spectra in the forward direction increases with Q^2 due to two body reactions[33] $\gamma_v p \to K^+ (\frac{\Lambda}{\Sigma})$, $K^+ Y^+$. No systematic study of $K^\pm$ spectra as a function of X has yet been made.

4.3.3. Proton Spectra: The yield at backward going protons $X < .5$ is shown in Fig. 27. The backward peak at $Q^2 = 0$ from $\gamma p \to (\rho\omega) + p$ disappears with increasing Q^2.

The model of Drell, Levy and Yan[34] assuming spin 1/2 partons inside protons thus predicts the forward proton yield should increase with Q^2 is not yet observed at DESY energies (Fig. 28).

* * *

ACKNOWLEDGEMENT

I wish to thank Dr. T. McCorriston, Dr. M. Della-Negra and Prof. A. Zichichi for many interesting conversations and for having provided me with useful data.

* * *

REFERENCES

1) S. Tavernier, Laboratoire de l'Accelerateur lineaire, Orsay, Report No. Rl 68/7, (1968)

2) R. Madaras et al. P.R.L. 30, p. 507 (1973)

3) V. Alles-Borelli et al. Nuovo Cimento, Vol. 7A, p. 345 (1972)

4) M. Bernardini et al., Submitted to Physics Letters, 1973.

B. Borgia et al. Nuovo Cimento letters, Vol. 3, p. 115 (1972)

5) T. D. Lee and G. C. Wick, Nucl. Phys. 9B, 209 (1969)

6) V. Alles-Borelli et al., Nuovo Cimento, Vol. 7, p. 330 (1972)

7) J. E. Augustin et al., P.R.L., Vol. 30, p. 462 (1973)

8) G. Jarlskog et al., DESY 73/4 (1973)

9 H. Cheng and T. T. Wu, P.R.L. 22, 666 (1969) and DESY 71/69

10) J. J. Sakurai, Ann. Phys. 11, 1 (1960)

11) H. Alvensleben et al., P.R.L. 27, 444 (1971)

12) J. le Francois, proceedings 1971, international symposium on Electron and Photon Interactions at High Energies, Cornell University, ed, by N. Mistry, p. 52

13) V. J. Auslander et al., P.L. 25B, 433 (1967)

14) H. Alvensleben et al. P.R.L. 27, 888 (1971)
H. Alvensleben et al. P.R.L. 28, 66 (1972)

15) H. Alvensleben et al. P.R.L. 26, 273 (1971)

16) G. Bacci et al., P.L. 38B, 551 (1972), G. Barbarino et al., lettre al Nuovo Cimento 3, 689 (1972)

17) H. H. Bingham et al., SLAC-Pub.-1113 and LBL-1085 (1972)

18) M. Bernardini et al. P.L. 44B, p. 393 (1973)

19) G. Barbiellini et al., I.N.F.N. report 420 (1973)

20) R. Kronig, J. Opt. Soc. Am. 12, 547 (1926), H. A. Kramers, Atti, Congr. intern. fisici, Como 2, 545 (1927)

21) M. Gell-Mann, M. C. Goldberger, W. Thirring, P.R. 95, 1612 (1954)

22) M. Damashek, F. J. Gilman, P.R. D1, 1319 (1970)
Also: T. A. Armstrong et al. P.R. D5, 1640 (1972)

23) S. J. Brodsky, J. G. Gillespie, P. R. 173, 1011 (1968)

24) J. Ballam et al., SLAC-pub-1143 (1972) and ref. therein

25) H. Alvensleben et al., P.R.L. 28, 66 (1972)

26) G. Wolf, DESY 72/61, E. D. Bloom et al. P.R.L. 23, 930 (1969)
M. Breidenbach et al. P.R.L. 23, 935 (1969)
G. Miller et al. P.R. D5, 528 (1972)

27) W. Albrecht et al. Nucl. Phys. B27, 615 (1971)

28) H. Cheng and T. T. Wu, P.R. 183, 1324 (1969); J. D. Bjorken, J. Kogut and D. Soper, P.R. D1, 1382 (1971), H. T. Nieh, P.L. B38, 100 (1972)

29) V. Eckardt et al., Proceedings of High Energy Physics Conference, Chicago 1972

30) ABBHHM Collaboration, P.R. 175, 1669 (1968)

31) L. Ahrens et al. (LNS 227, May 1973)

32) J. Ballam et al., M. Della-Negra, private communication

33) G. Wolf, DESY 72/61

34) S. D. Drell, D. J. Levy and T. M. Yan, P.R.L. 22, 744 (1969)

* * *

FIGURE CAPTIONS

Fig. 1 Layout of the by-pass on-line detector, showing a typical event.

Fig. 2 Experimental angular distribution of Bhabha scattering events compared with the normalized prediction of QED.

Fig. 3 S-dependence of $e^+e^- \to e^-e^+$ compared with QED, data from the CERN-Bologna-Frascati group.

Fig. 4 Results from Conversi group on $e^+e^- \to \mu^+\mu^-$ vs $e^+e^- \to e^-e^+$

Fig. 5 Results from the Zichichi group $\mu^+\mu^-/e^+e^-$ ratio accepted in the apparatus at various energies.

Fig. 6a Best fit of $e^+e^- \to \phi \to \mu^-\mu^+$ with the Kallen-Lehmann representation

Fig. 6b The excitation curve for $\phi \to K^-K^+$ for calibration

Fig. 7 Experimental set up of the DESY Delbrück experiment.

Fig. 8 Measured differential cross sections for Delbruck scattering vs t for Au compared with theory.

Fig. 9 Measured differential cross section for Delbrück scattering for U at small t

Fig. 10 Cross section of $\gamma+A \to A+\pi^-\pi^+$ from DESY/MIT. The solid line is fit with $\rho\omega$ interference. The other curves are a) no ω contribution, b) and c), d) backgrounds. See (Ref. 14)

Fig. 11 Mass spectra for $\gamma+c \to c+\pi^-\pi^+$ enhancement at 1.6 GeV is clearly seen.

Fig. 12 Cross section for $e^+e^- \to 2\pi^+2\pi^-$ for Ref. (16)

Fig. 13 $\gamma+p \to p+2\pi^+2\pi^-$ at 9.3 GeV, 4π mass spectrum. The shaded histogram has events with Δ^{++} removed

Fig. 14a Plan view of the spectrometer

Fig. 14b Difference between arrival times of e^- and e^+ for all detected pairs.

Fig. 14c Distribution of all events as a function of mass. The solid line is the theoretical prediction. The size of the vertical bars indicate the theoretical uncertainties. For m>20 MeV QED dominates and the theoretical uncertainties are negligible.

Fig. 15a Distribution of interference events as a function of mass. The solid line is the prediction of $d\sigma_{int}$

Fig. 15b Comparison of experimental results with dispersion relation prediction.

Fig. 16 Reaction $\gamma+p \to p\omega$. Total cross section as a function of the incident photon energy. The points labeled ABBHHM (P.R. 175, 1669 (1968)) and SLAC Annihilation Beam (P.R. D5, 15 (1972)) are earlier work. The full and dashed curves give the contributions of a diffractive process and OPE respectively.

Fig. 17 Reaction $\gamma+p \to \phi+p$

Fig. 18 Reaction $\gamma+p \to \phi+p$. Total cross section and exponential slope A of the differential cross section as function of incident photon energy.

Fig. 19 Total electroproduction cross section $\sigma_\tau^{tot} + \varepsilon\sigma_\tau^{tot}$, as a function of Q^2 for various W. Figure taken from G. Wolf, DESY 72/61.

Fig. 20 Total cross section for the reaction $ep \to ep\pi^+\pi^-$ as a function of the total hadron mass W for different Q^2 intervals, Ref. 26, ref.29, ref. 30.

Fig. 21 Reaction $ep \to ep+\pi^+\pi^-$; Q^2 dependence of the cross section for

different W intervals (ref. 29). The $Q^2 = 0$ points are from Ref. 30. Fig. taken from Ref. 29

Fig. 22 Measured slope of the t distribution for ρ^o and ω production plotted against the dimensionless inverse life time parameter $\frac{Q^2+m_p^2}{2m_\nu}$ Figure from Ref. 31.

Fig. 23 Average charged multiplicity vs ln W' from SLAC track chamber data.

Fig. 24 The normalized π^- yield for e $p \to e\pi^- + \ldots$ at W = 2.6 GeV and $Q^2=0$, and at $2.0<W<2.7$ GeV for different Q^2. The curve shows yield at $Q^2=0$ when $\gamma p \to p\rho^o$ are removed (Ref. 33, Fig. 28)

Fig. 25 Normalized π^- yield from 16 GeV SLAC track chamber data (Ref. 32)

Fig. 26 Normalized π^+ yield from 16 GeV SLAC track chamber data (Ref. 32)

Fig. 27 The normalized invariant cross sections for inclusive proton production for $x < -.5$ data from Ref. 32

Fig. 28 The normalized invariant cross sections for inclusive proton production at $P^2<0.02$ GeV^2, W = 2.63 GeV, $Q^2 = 0$ and $Q^2 = 1.16$ (Fig. from Ref. 33)

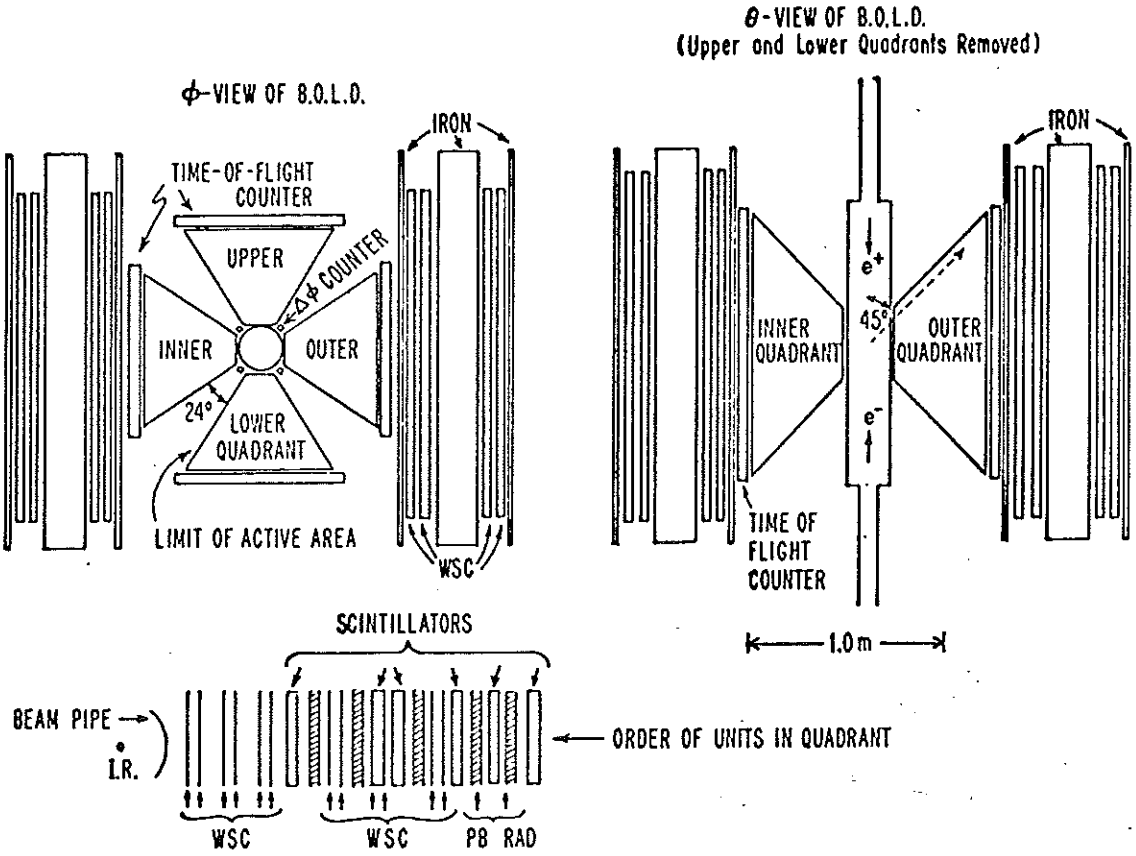
φ-VIEW OF B.O.L.D.
IRON
TIME-OF-FLIGHT COUNTER
UPPER
Δφ COUNTER
INNER
OUTER
24°
LOWER QUADRANT
LIMIT OF ACTIVE AREA
WSC
θ-VIEW OF B.O.L.D.
(Upper and Lower Quadrants Removed)
IRON
INNER QUADRANT
e+
45°
OUTER QUADRANT
e-
TIME OF FLIGHT COUNTER
1.0 m
SCINTILLATORS
BEAM PIPE
I.R.
ORDER OF UNITS IN QUADRANT
WSC
WSC
PB RAD

Fig. 1

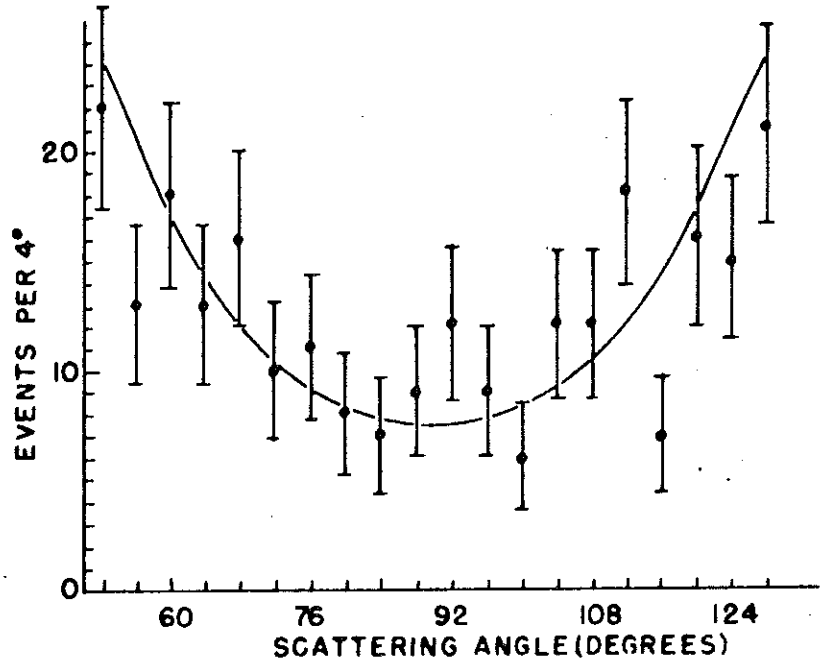

Fig. 2

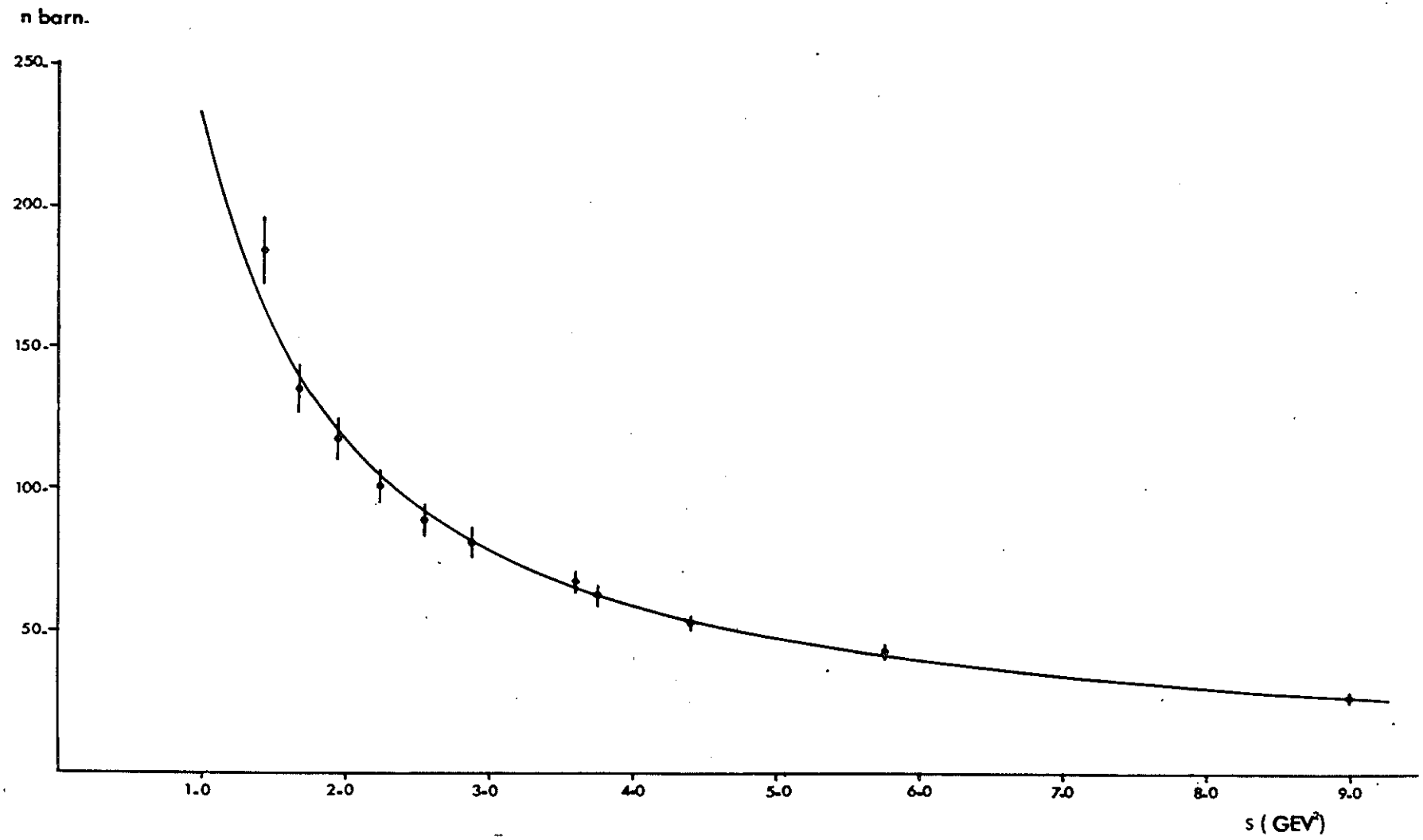

Fig. 3

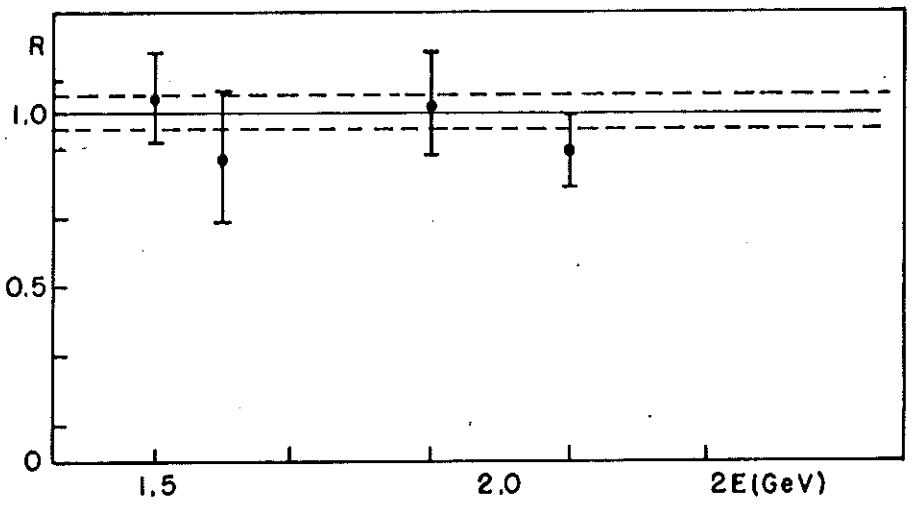
R
1.0
0.5
0
1.5
2.0
2E(GeV)

Fig. 4

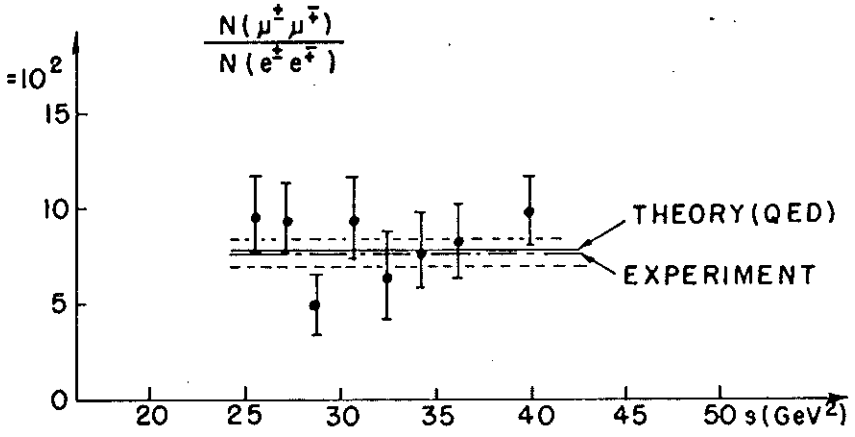
N(μ±μ∓)
N(e±e∓)
=10²
15
10
5
0
20
25
30
35
40
45
50 s(GeV²)
THEORY(QED)
EXPERIMENT

Fig. 5

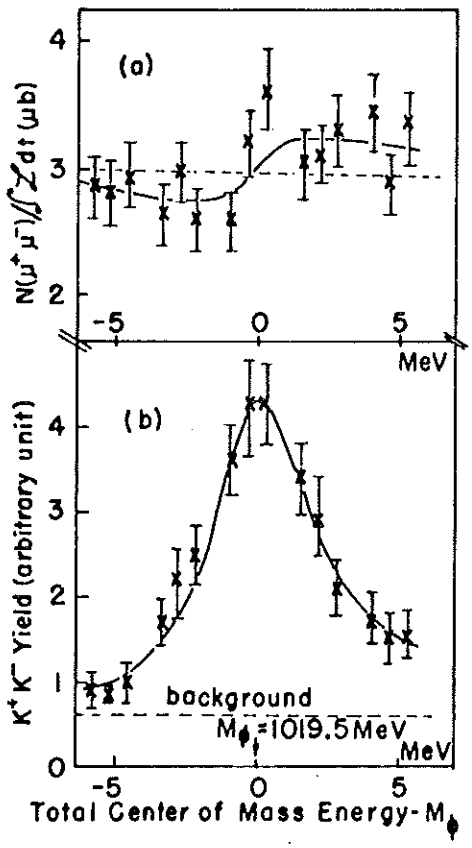
(a)
(b)
$N(\mu^+\mu^-)/\int \mathcal{L}\,dt$ (μb)
K^+K^- Yield (arbitrary unit)
background
M_ϕ=1019.5MeV
MeV
Total Center of Mass Energy-M_ϕ

Fig. 6

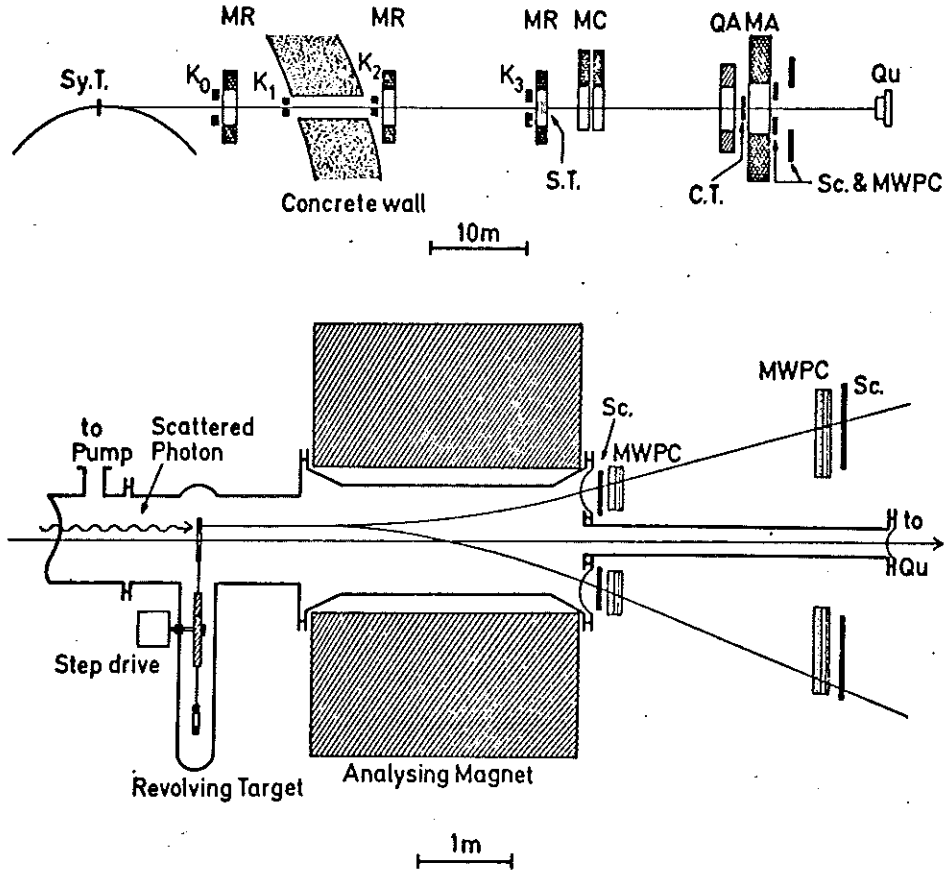
MR
MR
MR MC
QA MA
Sy.T.
K0
K1
K2
K3
Qu
S.T.
C.T.
Sc. & MWPC
Concrete wall
10m
MWPC
Sc.
Sc.
MWPC
to
Pump
Scattered
Photon
to
Qu
Step drive
Revolving Target
Analysing Magnet
1m

Fig. 7

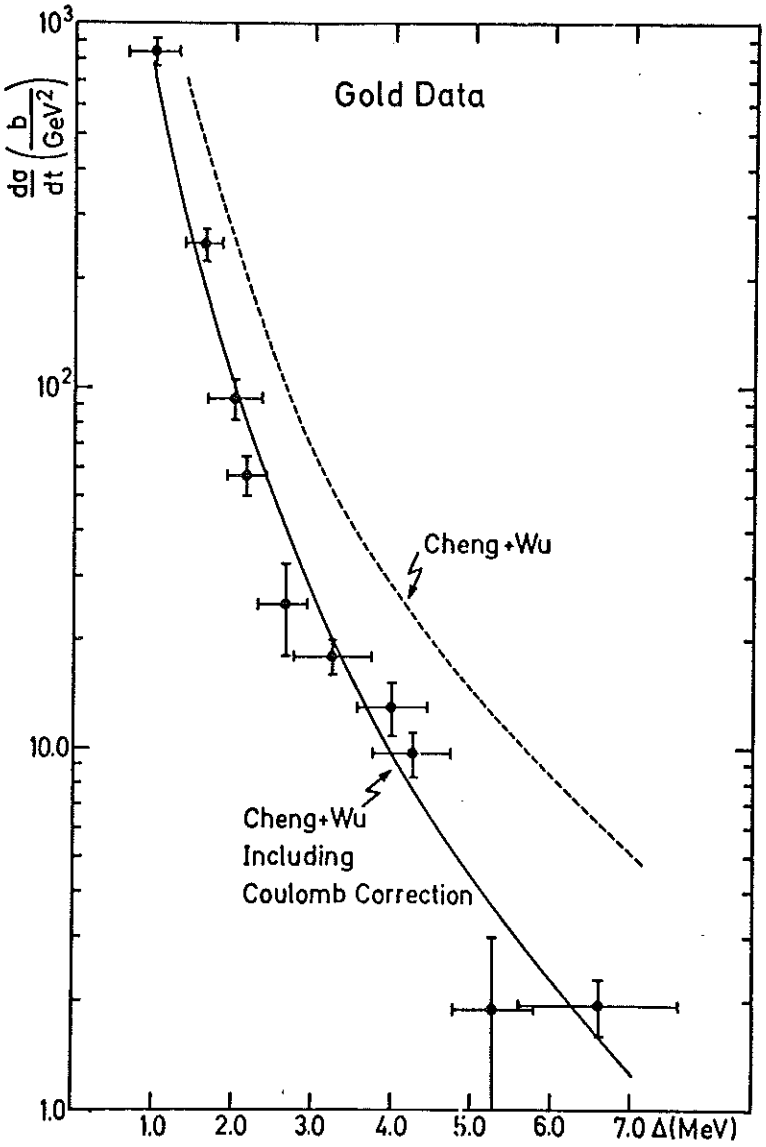
Gold Data
Cheng+Wu
Cheng+Wu
Including
Coulomb Correction
$\frac{d\sigma}{dt}\left(\frac{b}{GeV^2}\right)$
10^3
10^2
10.0
1.0
1.0
2.0
3.0
4.0
5.0
6.0
7.0 Δ(MeV)

Fig. 8

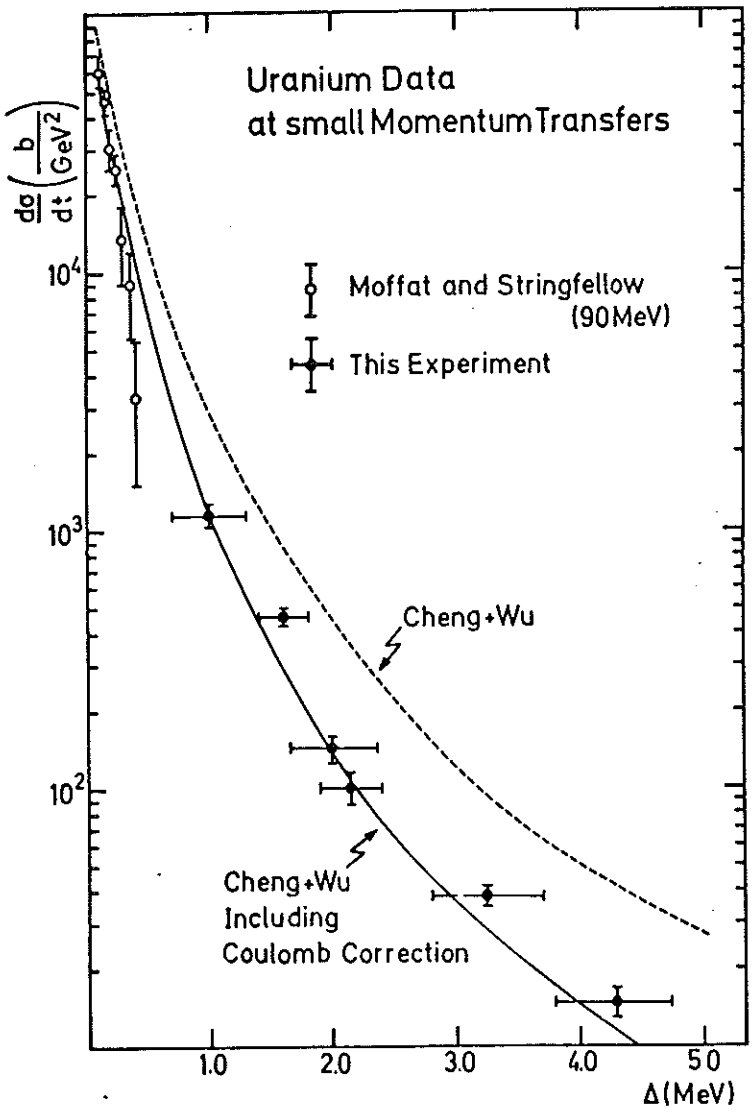
Uranium Data
at small Momentum Transfers
dσ/dt (b/GeV²)
10⁴
10³
10²
Moffat and Stringfellow
(90MeV)
This Experiment
Cheng+Wu
Cheng+Wu
Including
Coulomb Correction
1.0
2.0
3.0
4.0
5.0
Δ(MeV)

Fig. 9

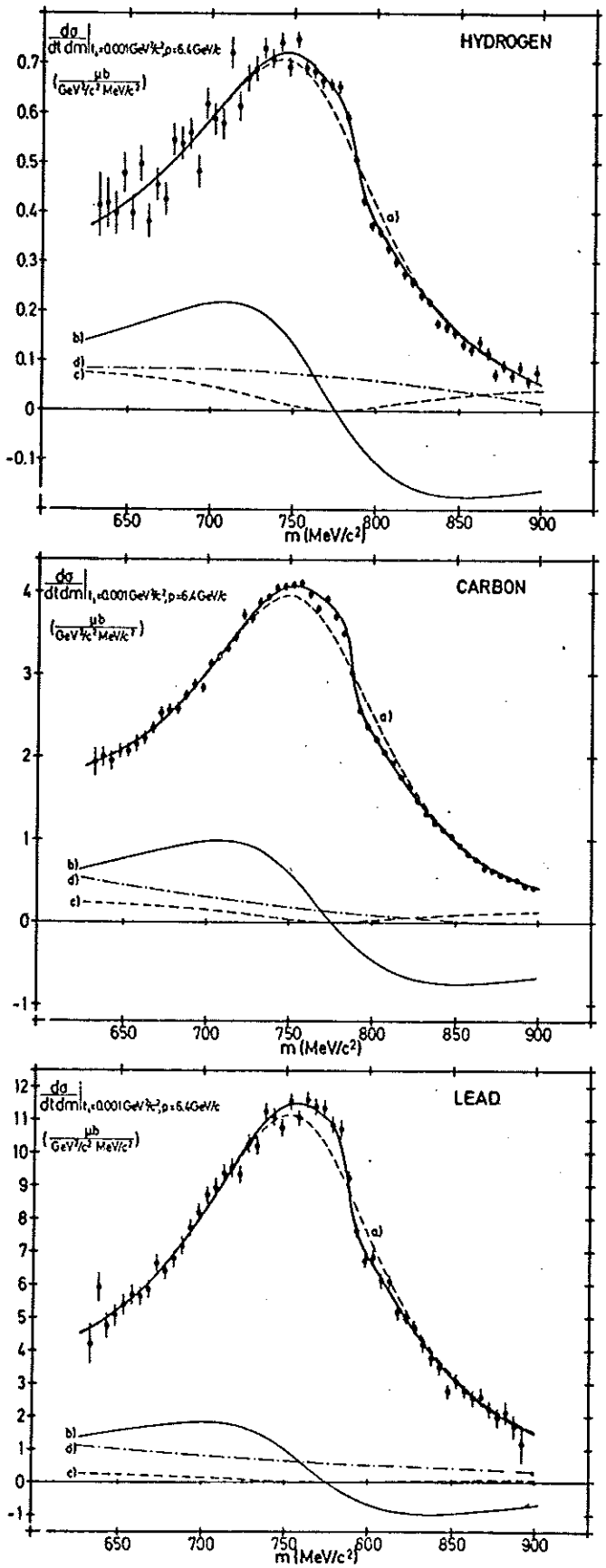

Fig. 10

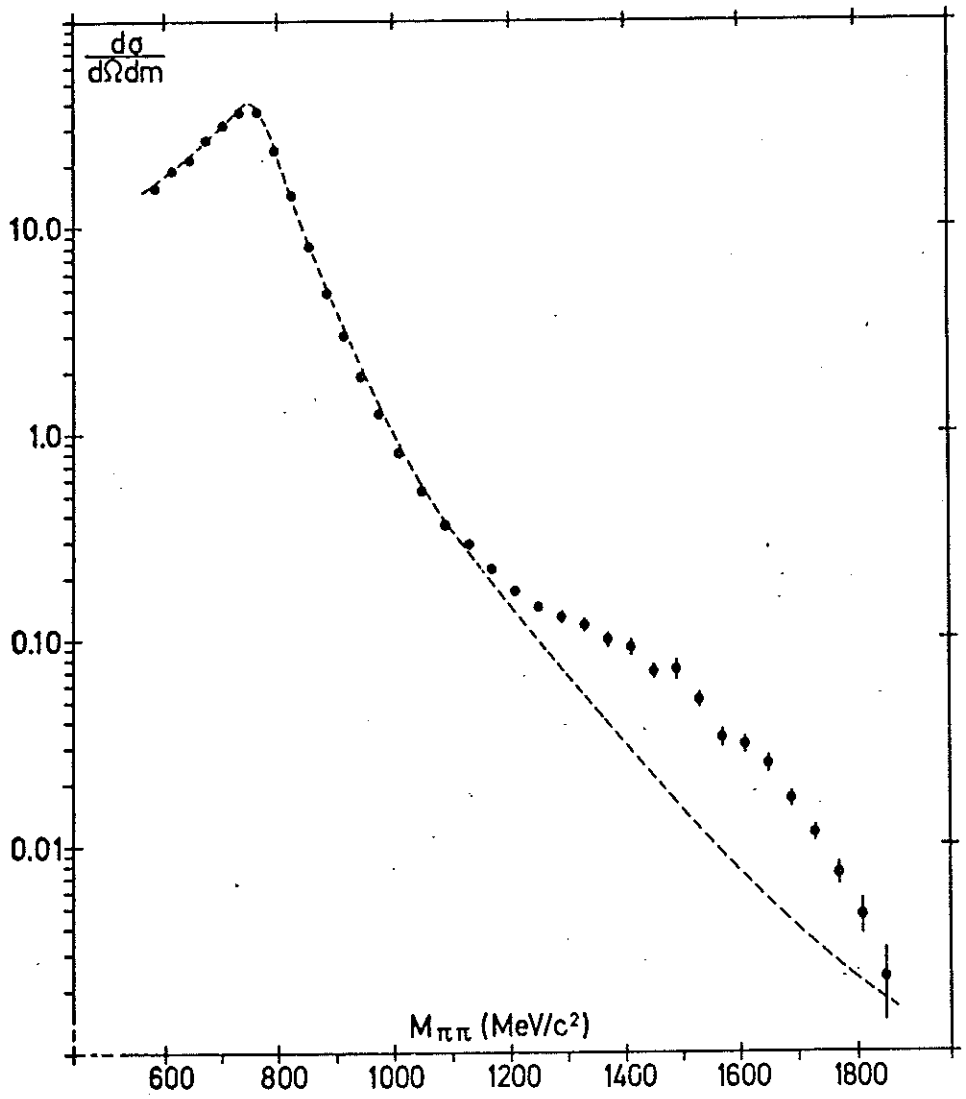
dσ/dΩdm
10.0
1.0
0.10
0.01
Mππ (MeV/c²)
600
800
1000
1200
1400
1600
1800

Fig. 11

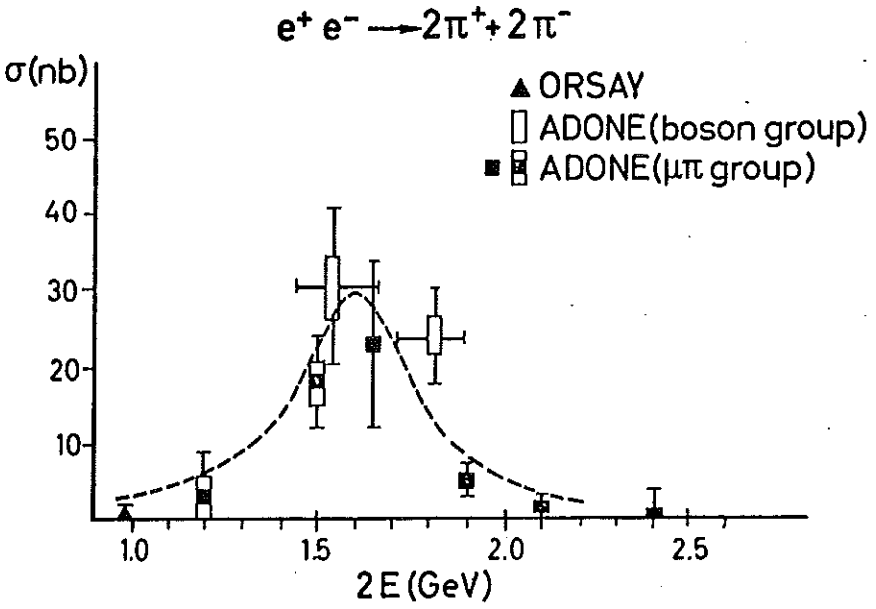
e+ e− ⟶ 2π+ + 2π−
σ(nb)
50
40
30
20
10
▲ ORSAY
▯ ADONE(boson group)
▯ ADONE(μπ group)
1.0
1.5
2.0
2.5
2E (GeV)

Fig. 12

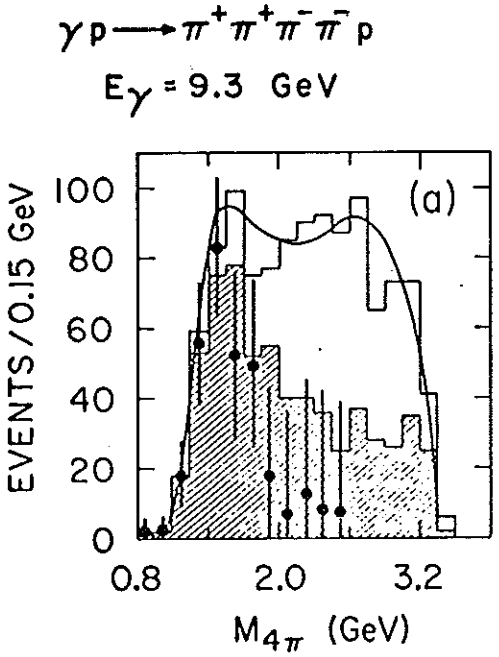
γ p ⟶ π+ π+ π− π− p
Eγ = 9.3 GeV
EVENTS / 0.15 GeV
100
80
60
40
20
0
(a)
0.8
2.0
3.2
M4π (GeV)

Fig. 13

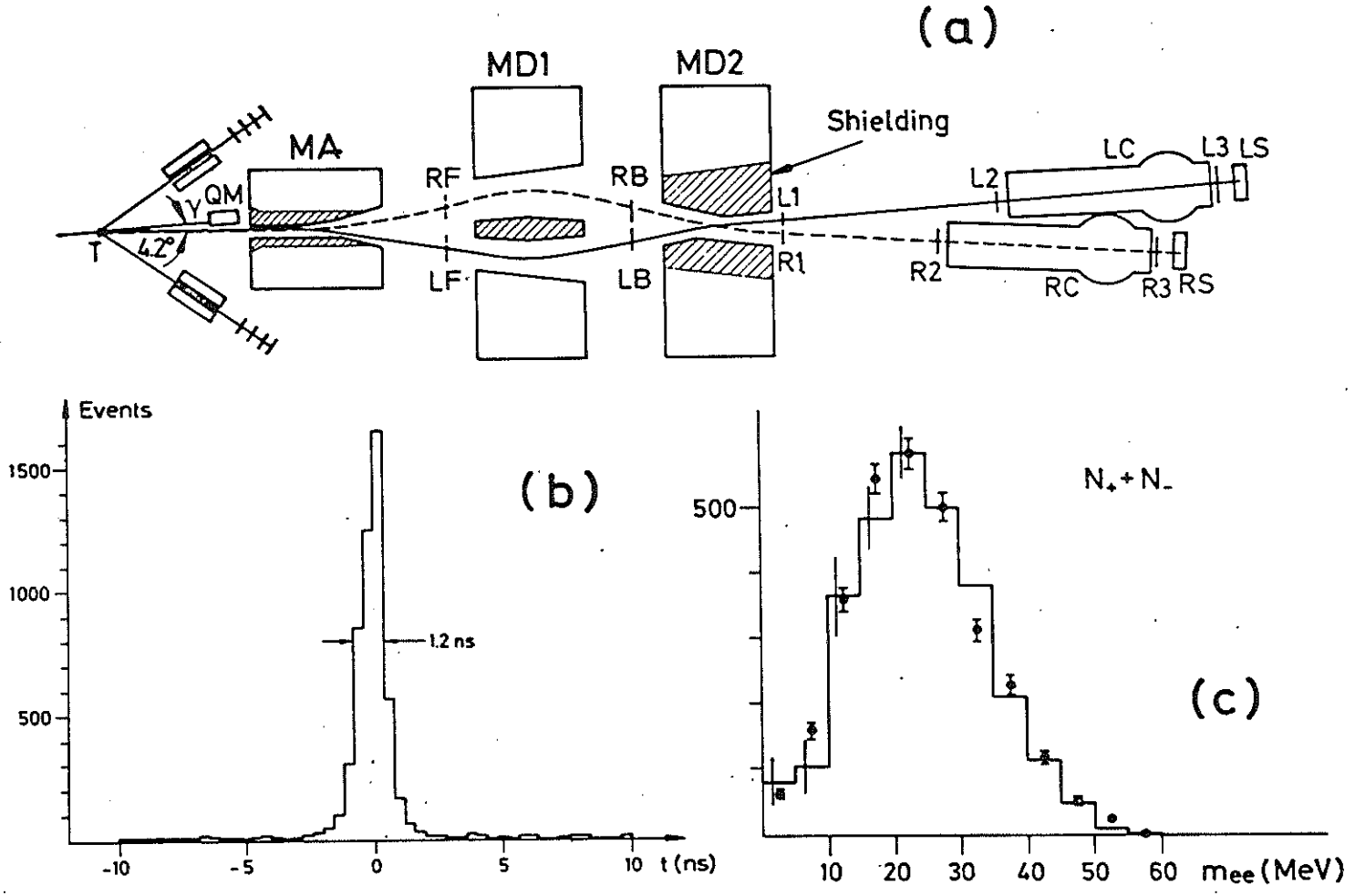
(a)
MD1
MD2
Shielding
MA
RF
RB
QM
Y
T
4.2°
LF
LB
L1
R1
L2
R2
LC
L3
LS
RC
R3
RS
Events
1500
1000
500
(b)
1.2 ns
-10
-5
0
5
10
t (ns)
N+ + N-
500
(c)
10
20
30
40
50
60
mee (MeV)

Fig. 14

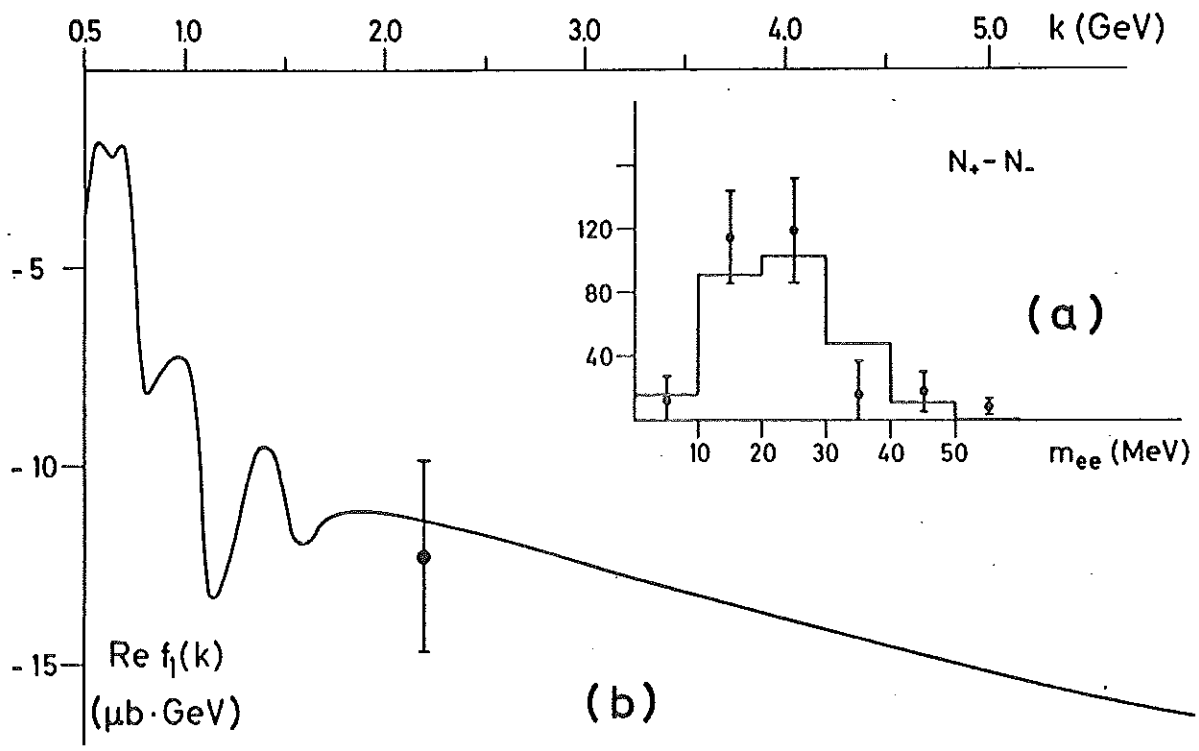
0.5
1.0
2.0
3.0
4.0
5.0
k (GeV)
-5
-10
-15
Re $f_1(k)$
(μb·GeV)
(b)
$N_+ - N_-$
120
80
40
(a)
10
20
30
40
50
m_{ee} (MeV)

Fig. 15

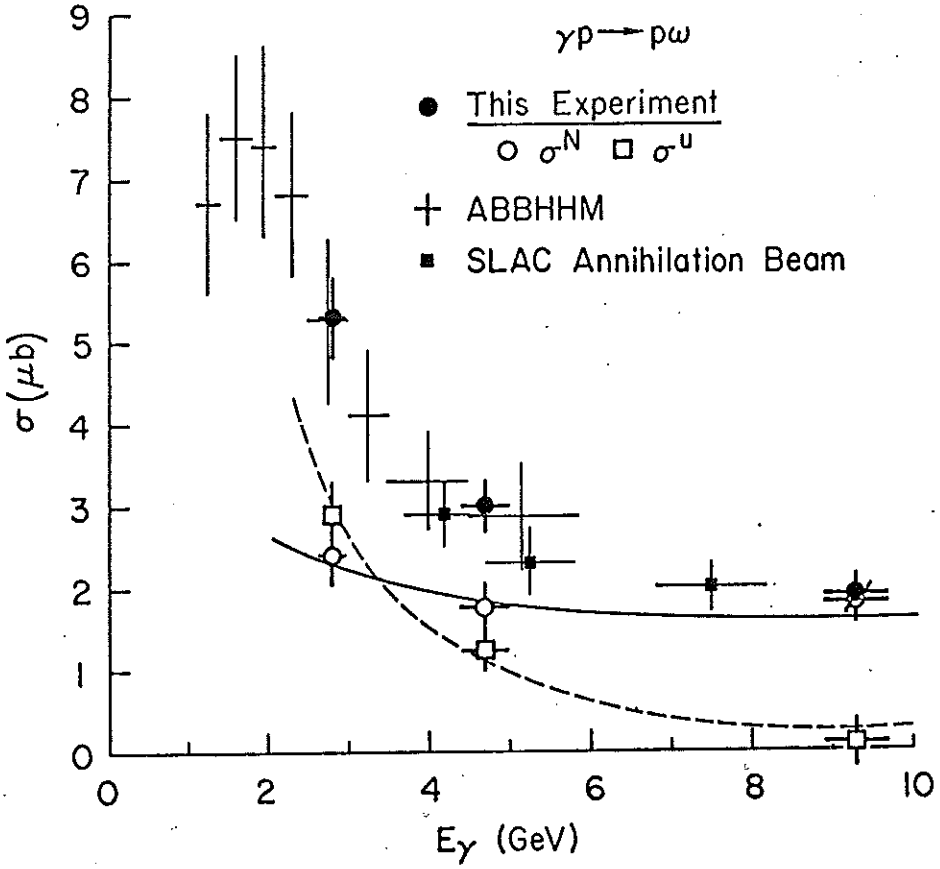
γp → pω
This Experiment
σ^N σ^u
ABBHHM
SLAC Annihilation Beam
σ (μb)
Eγ (GeV)
0
1
2
3
4
5
6
7
8
9
0
2
4
6
8
10

Fig. 16

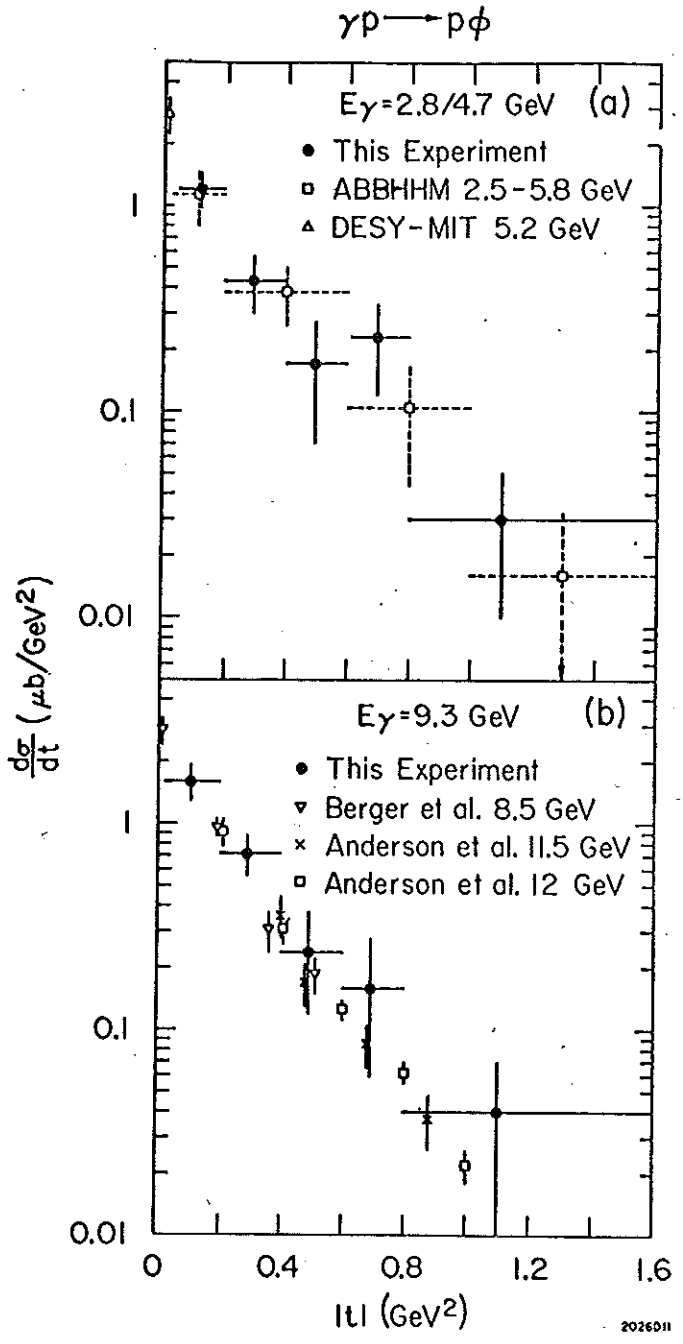
γp → pφ
Eγ=2.8/4.7 GeV (a)
This Experiment
ABBHHM 2.5-5.8 GeV
DESY-MIT 5.2 GeV
Eγ=9.3 GeV (b)
This Experiment
Berger et al. 8.5 GeV
Anderson et al. 11.5 GeV
Anderson et al. 12 GeV
dσ/dt (μb/GeV²)
1
0.1
0.01
0
0.4
0.8
1.2
1.6
|t| (GeV²)
2026011

Fig. 17

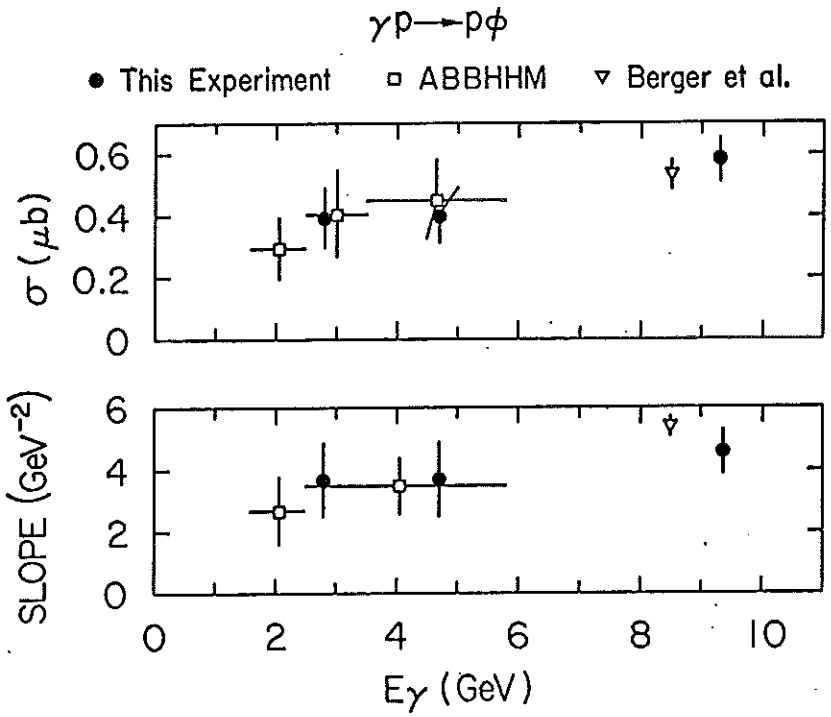
γp→pφ
● This Experiment
□ ABBHHM
▽ Berger et al.
σ (μb)
0.6
0.4
0.2
0
SLOPE (GeV⁻²)
6
4
2
0
0
2
4
6
8
10
Eγ (GeV)

Fig. 18

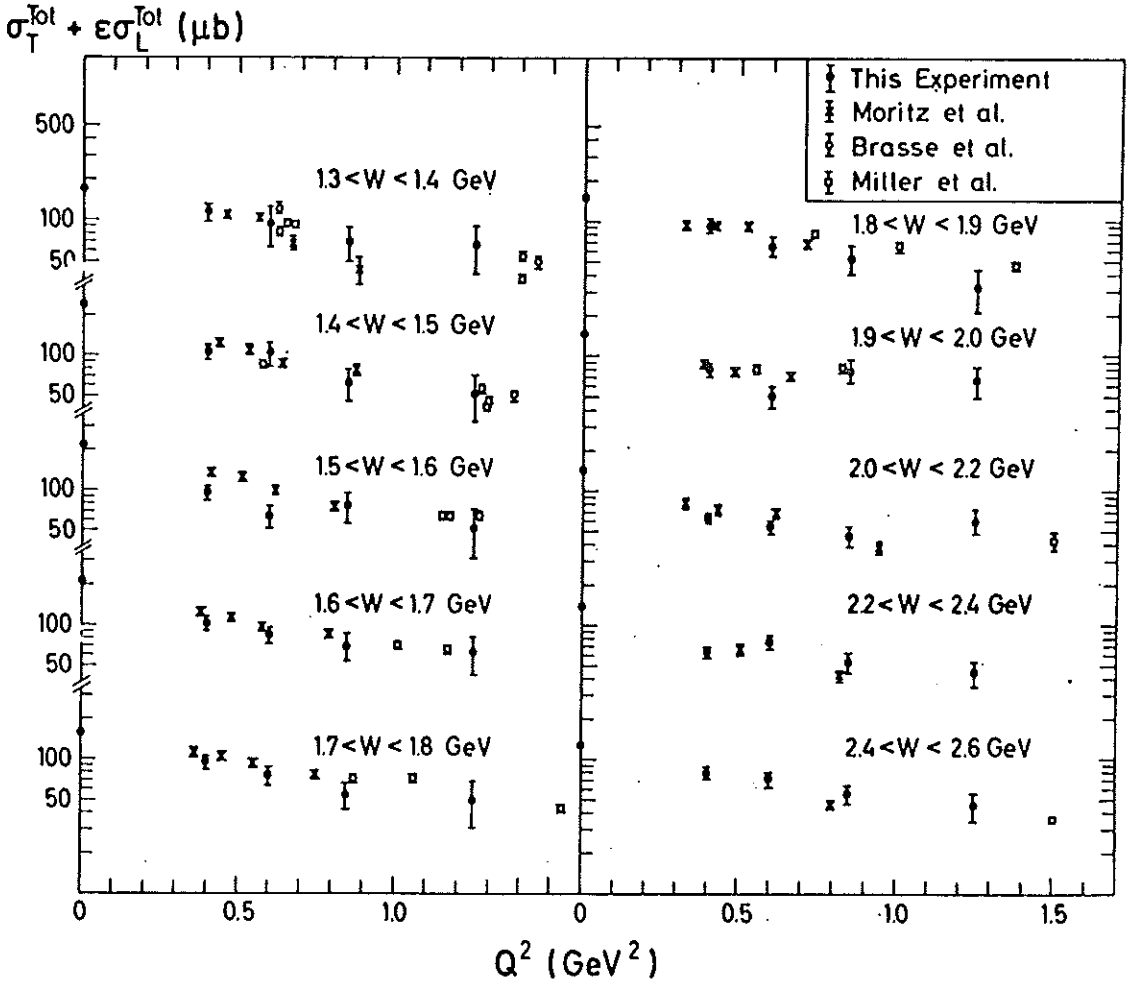
$\sigma_T^{Tot} + \varepsilon\sigma_L^{Tot}$ (μb)
This Experiment
Moritz et al.
Brasse et al.
Miller et al.
1.3<W<1.4 GeV
1.4<W<1.5 GeV
1.5<W<1.6 GeV
1.6<W<1.7 GeV
1.7<W<1.8 GeV
1.8<W<1.9 GeV
1.9<W<2.0 GeV
2.0<W<2.2 GeV
2.2<W<2.4 GeV
2.4<W<2.6 GeV
500
100
50
0
0.5
1.0
1.5
Q^2 (GeV^2)

Fig. 19

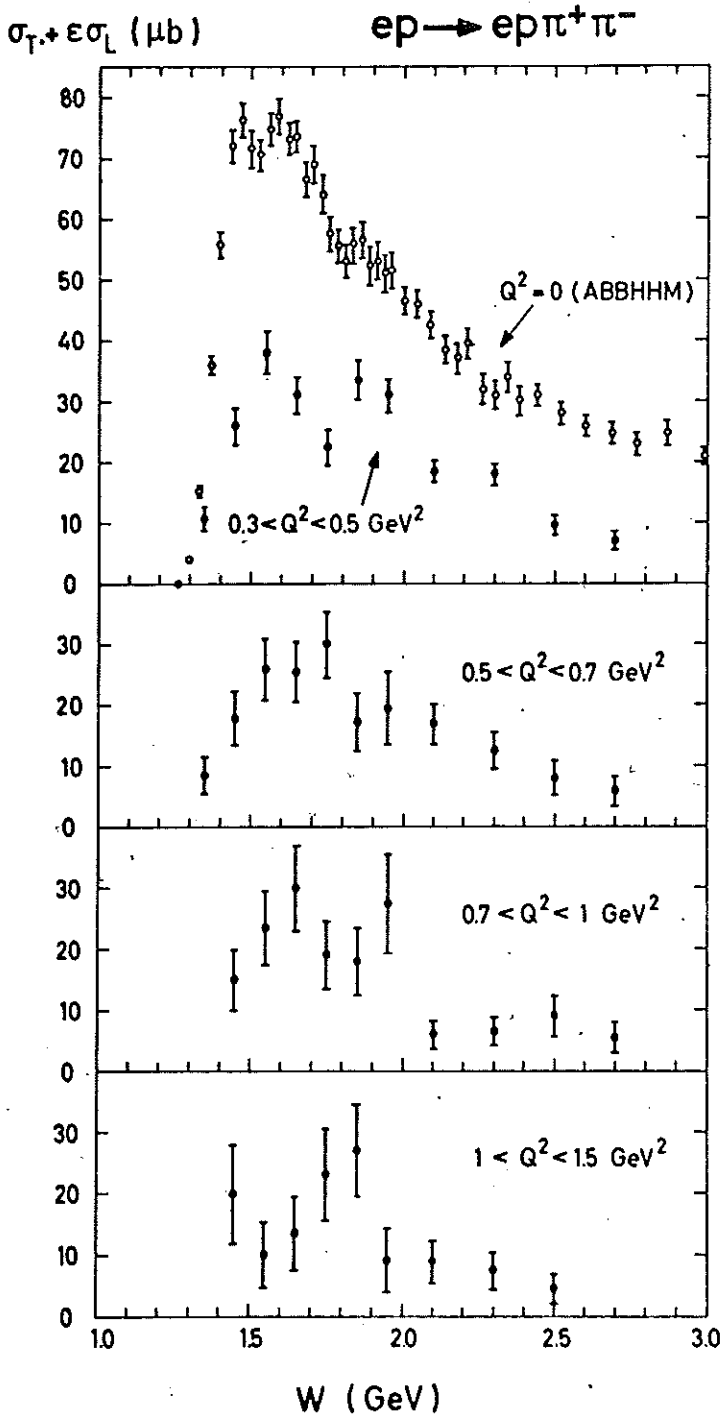
$\sigma_{T.} + \varepsilon\sigma_L$ (μb)
$ep \longrightarrow ep\pi^+\pi^-$
$Q^2 = 0$ (ABBHHM)
$0.3 < Q^2 < 0.5$ GeV^2
$0.5 < Q^2 < 0.7$ GeV^2
$0.7 < Q^2 < 1$ GeV^2
$1 < Q^2 < 1.5$ GeV^2
W (GeV)

Fig. 20

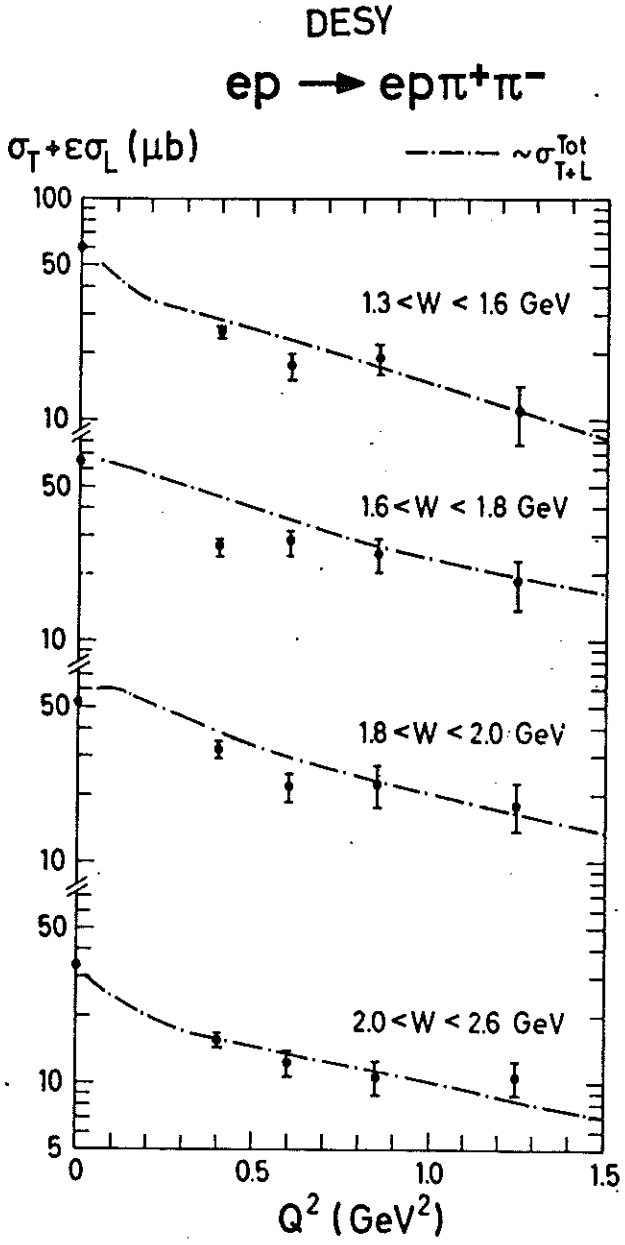
DESY
ep → epπ⁺π⁻
σT+εσL (μb)
~σ Tot T+L
100
50
10
50
10
50
10
50
10
5
1.3<W < 1.6 GeV
1.6<W < 1.8 GeV
1.8<W < 2.0 GeV
2.0<W < 2.6 GeV
0
0.5
1.0
1.5
Q² (GeV²)

Fig. 21

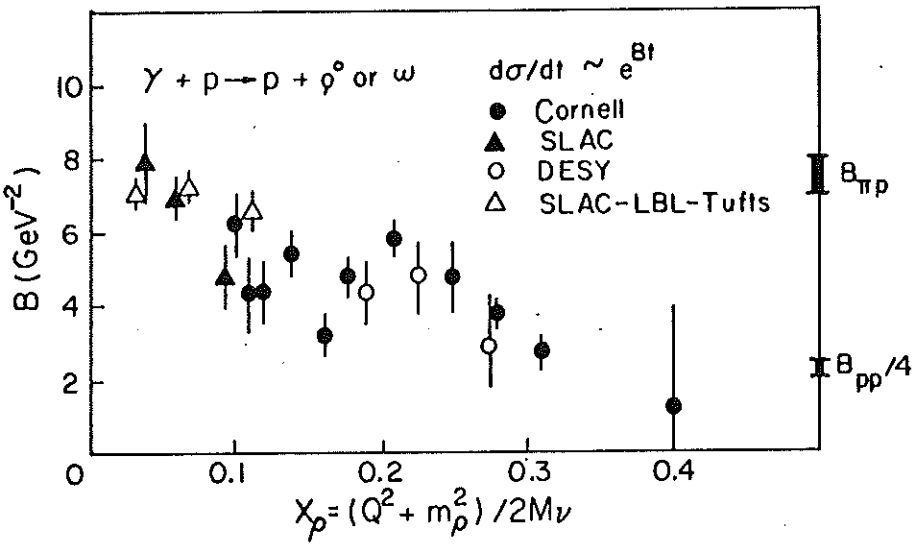
γ + p → p + ρ° or ω
dσ/dt ~ e^Bt
Cornell
SLAC
DESY
SLAC-LBL-Tufts
B (GeV^-2)
B_πp
B_pp/4
X_p = (Q^2 + m_ρ^2) /2Mν

Fig. 22

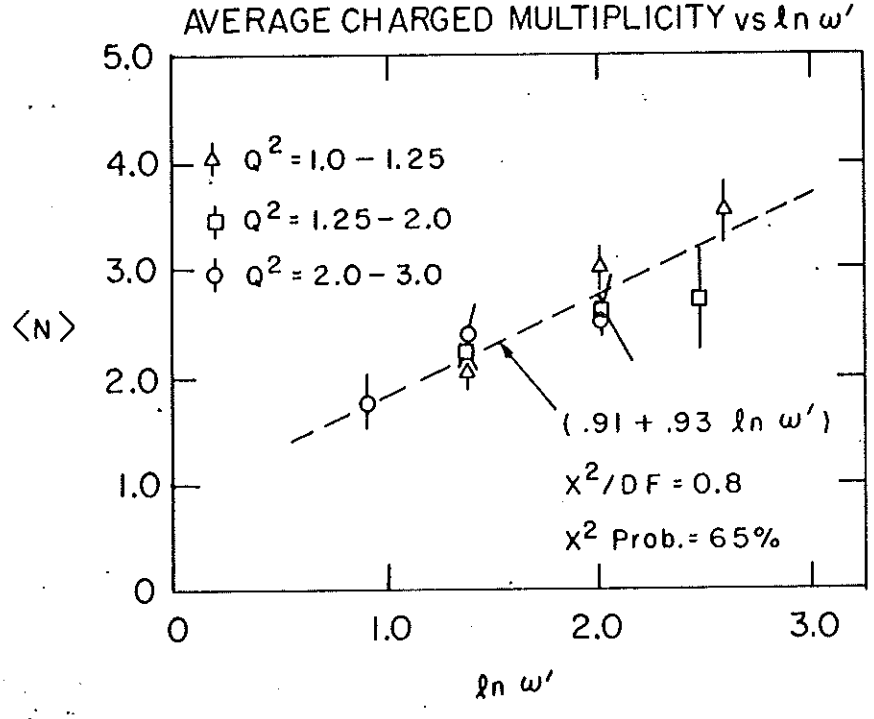
AVERAGE CHARGED MULTIPLICITY vs ln ω'
Q^2 = 1.0 – 1.25
Q^2 = 1.25 – 2.0
Q^2 = 2.0 – 3.0
⟨N⟩
(.91 + .93 ln ω')
X^2/DF = 0.8
X^2 Prob. = 65%
ln ω'

Fig. 23

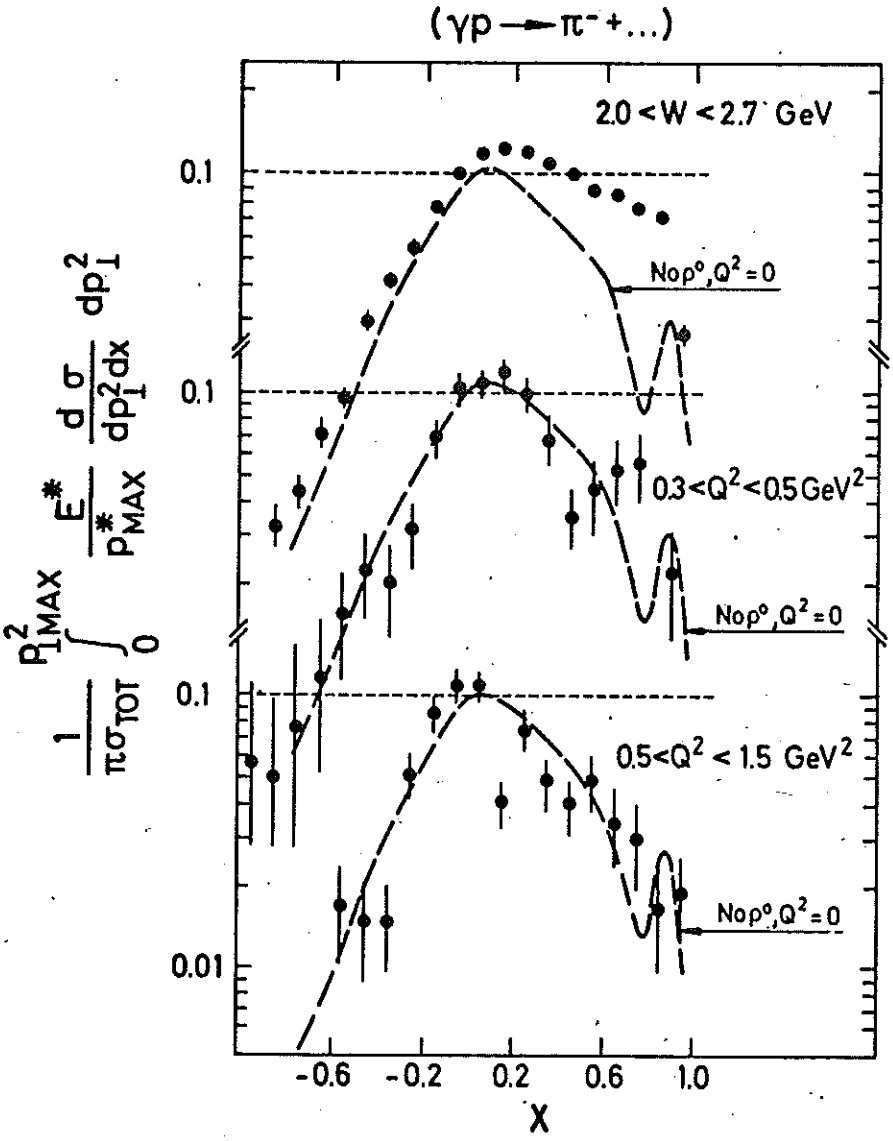
(γp → π⁻ + ...)
2.0 < W < 2.7 GeV
0.1
No ρ°, Q² = 0
0.1
0.3 < Q² < 0.5 GeV²
No ρ°, Q² = 0
0.1
0.5 < Q² < 1.5 GeV²
No ρ°, Q² = 0
0.01
-0.6
-0.2
0.2
0.6
1.0
X
$\frac{1}{\pi\sigma_{TOT}} \int_0^{P_{T\,MAX}^2} \frac{E^*}{p^*_{MAX}} \frac{d\sigma}{dp_T^2 dx} dp_T^2$

Fig. 24

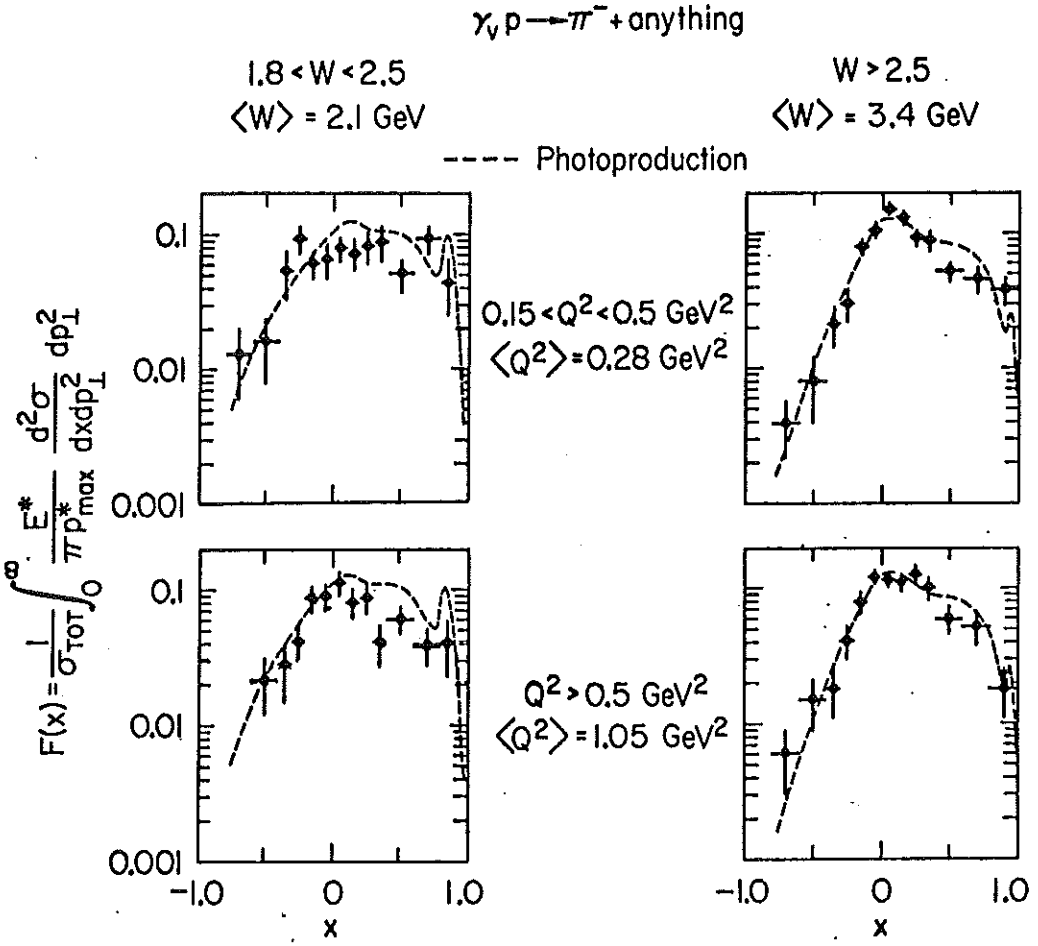
$\gamma_v p \rightarrow \pi^- +$ anything
1.8 < W < 2.5
⟨W⟩ = 2.1 GeV
W > 2.5
⟨W⟩ = 3.4 GeV
---- Photoproduction
$F(x) = \frac{1}{\sigma_{TOT}} \int_0^\infty \frac{E^*}{\pi p^*_{max}} \frac{d^2\sigma}{dx dp_\perp^2} dp_\perp^2$
0.15 < Q² < 0.5 GeV²
⟨Q²⟩ = 0.28 GeV²
Q² > 0.5 GeV²
⟨Q²⟩ = 1.05 GeV²
0.1
0.01
0.001
-1.0
0
1.0
x

Fig. 25

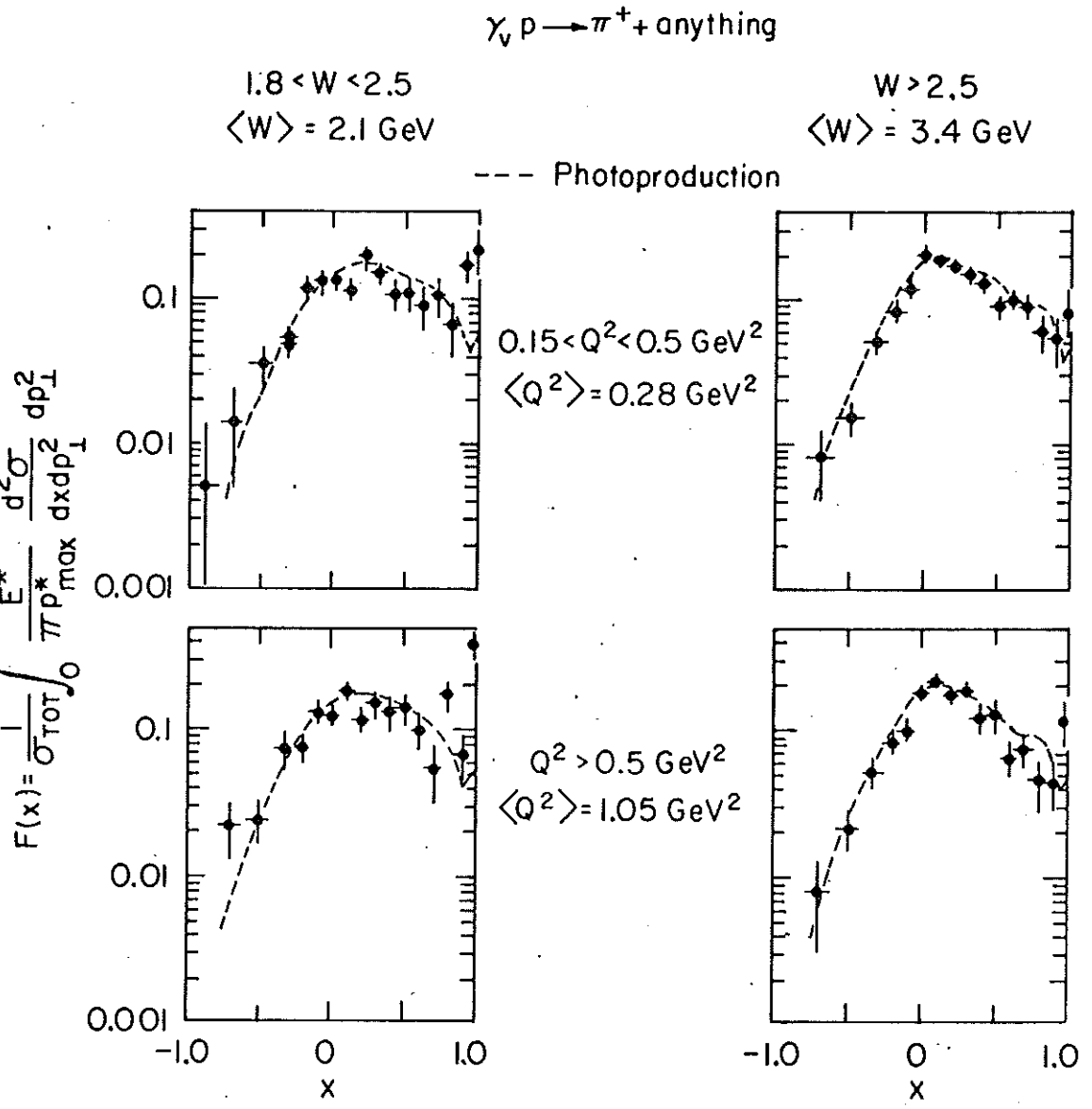
$\gamma_v p \rightarrow \pi^+ +$ anything
1.8 < W < 2.5
⟨W⟩ = 2.1 GeV
W > 2.5
⟨W⟩ = 3.4 GeV
--- Photoproduction
$F(x) = \frac{1}{\sigma_{TOT}} \int_0^\infty \frac{E^*}{\pi p^*_{max}} \frac{d^2\sigma}{dx\,dp_\perp^2}\, dp_\perp^2$
0.15 < Q² < 0.5 GeV²
⟨Q²⟩ = 0.28 GeV²
Q² > 0.5 GeV²
⟨Q²⟩ = 1.05 GeV²
0.1
0.01
0.001
-1.0
0
1.0
x

Fig. 26

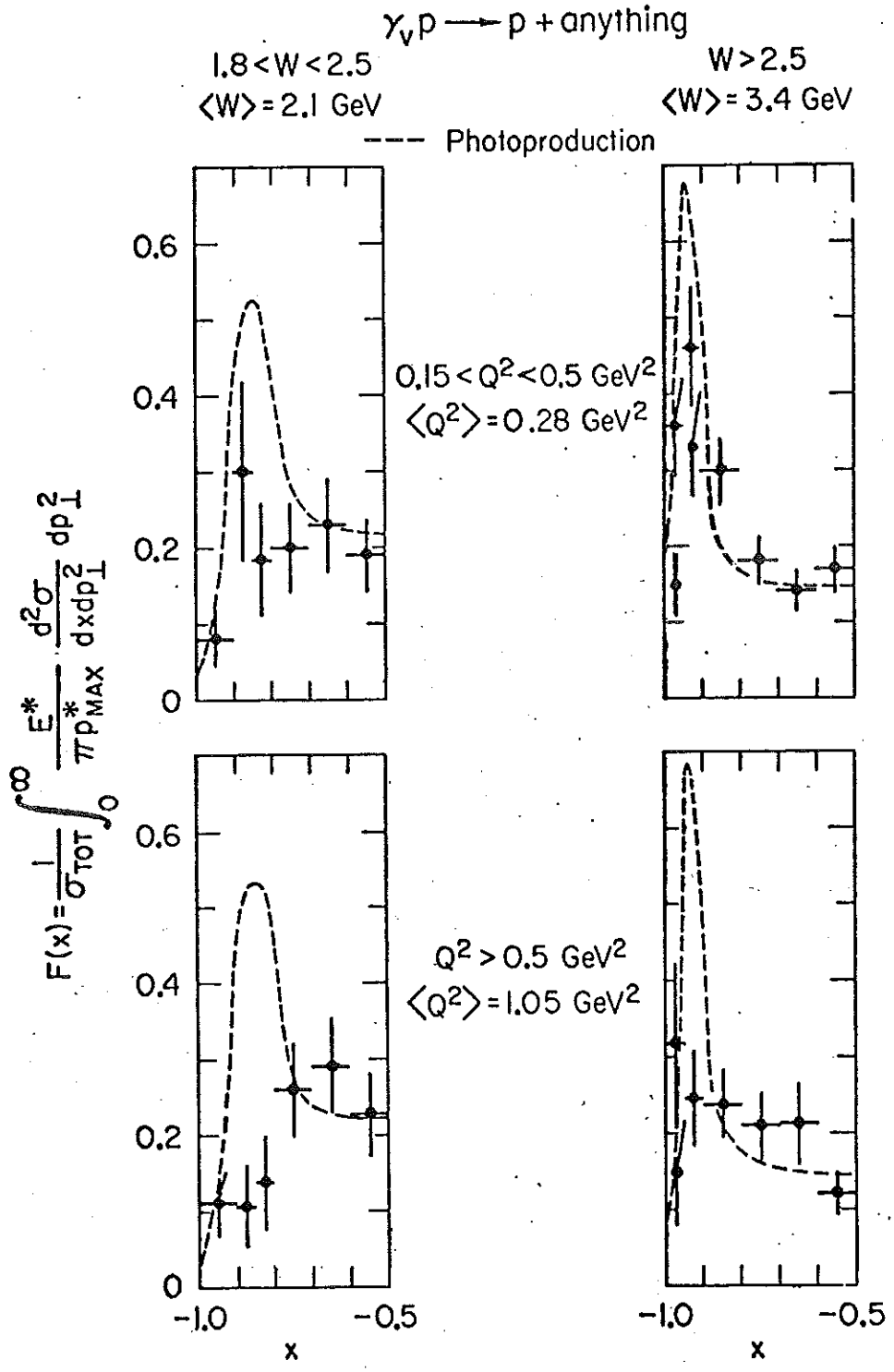
$\gamma_v p \longrightarrow p + \text{anything}$
1.8<W<2.5
⟨W⟩ = 2.1 GeV
W>2.5
⟨W⟩ = 3.4 GeV
--- Photoproduction
0.15<Q²<0.5 GeV²
⟨Q²⟩ = 0.28 GeV²
Q² > 0.5 GeV²
⟨Q²⟩ = 1.05 GeV²
$F(x) = \frac{1}{\sigma_{TOT}} \int_0^\infty \frac{E^*}{\pi p^*_{MAX}} \frac{d^2\sigma}{dx dp_T^2} dp_T^2$
0.6
0.4
0.2
0
-1.0
-0.5
x

Fig. 27

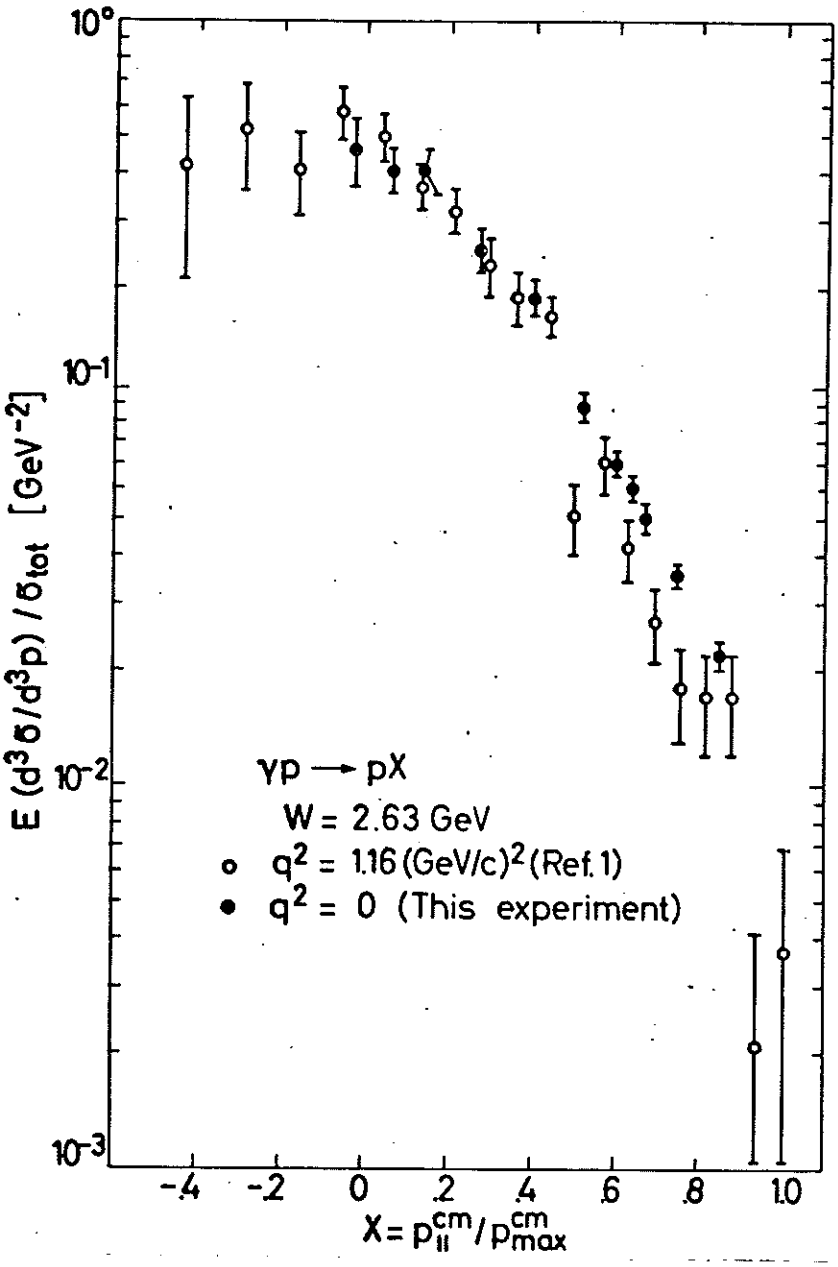
10°
10⁻¹
10⁻²
10⁻³
E (d³σ/d³p) / σtot [GeV⁻²]
γp → pX
W = 2.63 GeV
q² = 1.16 (GeV/c)² (Ref. 1)
q² = 0 (This experiment)
-.4
-.2
0
.2
.4
.6
.8
1.0
X = p_II^cm / p_max^cm

Fig. 28